

# A Wavelet Based Space-Time Adaptive Numerical Method for Partial Differential Equations

*Emmanuel Bacry, Stéphane Mallat<sup>1</sup> and George Papanicolaou*

Courant Institute of Mathematical Sciences  
New York University  
251 Mercer Street  
New York, NY 10012, USA

## Abstract

We describe a space and time adaptive numerical method based on wavelet orthonormal bases for solving partial differential equations. The multiresolution structure of wavelet orthonormal bases provides a simple way to adapt computational refinements to the local regularity of the solution [11] [16]. High resolution computations are performed only in regions where singularities or sharp transitions occur. For many evolution equations it is necessary to adapt the time steps to the spatial resolution in order to maintain the stability and precision of the numerical scheme. We describe an algorithm that modifies the time discretization at each resolution, depending on the structure of the solution. The stability of this space-time adaptive scheme is studied for the heat equation and the linear advection equation. We also explain how this algorithm can be used to solve the one-dimensional Burgers equation with periodic boundary conditions. We present numerical results on the accuracy and complexity of the algorithm.

---

<sup>1</sup>This research was supported by the AFOSR grant AFOSR-90-0040.

# 1 Introduction.

Singularities and sharp transitions in solutions of partial differential equations model important physical phenomena such as beam focusing in nonlinear optics, the formation of shock waves in compressible gas flow, the formation of vortex sheets in high Reynolds number incompressible flows, etc. A characteristic feature of such phenomena is that the complex behavior occurs in a small region of space and intermittently in time. This makes them particularly hard to simulate numerically by solving the partial differential equations with conventional numerical methods, prompting the development of adaptive numerical methods. In these methods most of the computational effort is concentrated near regions where singularities or sharp transitions occur. We will study here a numerical method for solving partial differential equations based on the wavelet transform, which is adaptive both in space and time.

Adaptive grids have been studied extensively in numerical analysis. Adaptive finite element methods have been proposed by Brandt [7] for elliptic problems, and developed by Bank [1] and others. More recently, Berger and Olinger [4] have studied and implemented an adaptive mesh refining method for hyperbolic partial differential equations which has been successful in solving previously intractable problems [3]. They use a sequence of nested grids in space that are progressively finer. An automatic error estimation step determines locally whether the current resolution of the numerical solution is sufficient or a finer grid is necessary. The main difficulty is finding stable and accurate difference approximations of the differential operators at the interfaces between grids of different sizes.

A non-orthogonal hierarchical basis method has been proposed by Yserentant [19] to adapt the numerical computations to the local regularity of the solution. Wavelets orthogonal bases are other examples of hierarchical bases. Liandrat and Tchamitchian [11] and Perrier and Basdevant [16] have shown that the multiresolution structure of wavelet orthonormal bases is a simple and effective framework for spatial adaptive algorithms. Instead of refining the computations through nested grids of successively finer meshes, as in the algorithm of Berger and Olinger [4], wavelet orthonormal bases implement adaptive refinement by successively adding layers of “details” that increase the resolution of the approximation locally. Communication between the different layers of details is regulated automatically by the orthogonality of the basis functions. The order of approximation of this spatial discretization depends upon the wavelet that is used.

In Section 2, we review briefly the construction of wavelet orthonormal bases through multiresolution approximations. In Section 3, we describe the Liandrat-Tchamitchian, Perrier-Basdevant spatial adaptive scheme for solving partial differential equations. For many evolution problems that are solved numerically with a space adaptive scheme, it is necessary to adapt the time discretization to the spatial resolution. If we use a time step  $\Delta t$ , it must be adapted to the highest resolution that is encountered over the whole spatial domain, even if this high resolution is maintained over a very small domain. If the spatial resolution is refined locally, the time step  $\Delta t$  must also be refined to maintain the stability and accuracy of the numerical scheme. This means that a local spatial refinement, even over a small domain, increases the global numerical complexity quite substantially. To avoid this problem, Berger and Olinger [4] have introduced local time steps that are adapted to the local mesh refinements. For adaptive numerical methods based on wavelets, it is also important to have a local time discretization. In this paper we present a new algorithm that adapts the time discretization to the resolution parameter that appears in a wavelet orthonormal basis. We describe this algorithm in Section 4, first for the heat equation and then for the linear advection equation. We have studied numerically the stability of the algorithm in these two cases. In Section 5 we describe how this algorithm can be applied to Burgers equation and we present some numerical results.

## 2 Multiresolution Approximations and Wavelets.

Wavelet orthonormal bases were introduced by Meyer [14] and Stromberg [17]. These bases are built from a single function  $\psi(x)$  which is dilated and translated on uniform grids. Let

$$\psi_j(x) = \sqrt{2^j} \psi(2^j x) \quad (1)$$

and

$$\psi_{j,n}(x) = \psi_j(x - 2^{-j}n). \quad (2)$$

Then, for certain functions  $\psi(x)$ , the sequence of functions  $(\psi_{j,n}(x))_{(n,j) \in \mathbb{Z}^2}$ , is an orthonormal basis in  $\mathbf{L}^2(\mathbf{R})$ . A good way to understand the construction of wavelet orthonormal bases is through the multiresolution analysis introduced by Meyer [14] and Mallat [13]. The approximation of a function  $f(x) \in \mathbf{L}^2(\mathbf{R})$  at the resolution  $2^j$  is defined as the orthogonal projection of  $f(x)$  on a space  $\mathbf{V}_j$  of a multiresolution approximation.

**Definition.** A multiresolution approximation of  $\mathbf{L}^2(\mathbf{R})$  is a sequence  $(\mathbf{V}_j)_{j \in \mathbb{Z}}$  of closed sub-spaces of  $\mathbf{L}^2(\mathbf{R})$  such that:

1.  $\forall j \in \mathbb{Z}, \mathbf{V}_{j-1} \subset \mathbf{V}_j$
2.  $\bigcap_{j=-\infty}^{+\infty} \mathbf{V}_j = \{0\}$
3.  $\bigcup_{j=-\infty}^{+\infty} \mathbf{V}_j = \mathbf{L}^2(\mathbf{R})$
4.  $\forall f \in \mathbf{L}^2(\mathbf{R}), \forall j \in \mathbb{Z}, f(x) \in \mathbf{V}_j \iff f(2x) \in \mathbf{V}_{j+1}$
5. There exists a function  $g(x) \in \mathbf{V}_0$  such that the sequence  $(g(x - n))_{n \in \mathbb{Z}}$  is a Riesz basis of  $\mathbf{V}_0$ .

It can be shown that for any multiresolution approximation there exists a function  $\phi \in \mathbf{V}_0$ , called scaling function, such that if we denote

$$\phi_j(x) = \sqrt{2^j} \phi(2^j x) \quad (3)$$

and

$$\phi_{j,n}(x) = \phi_j(x - 2^{-j}n), \quad (4)$$

then at any resolution  $2^j$ , the family of functions  $(\phi_{j,n}(x))_{n \in \mathbb{Z}}$ , is an orthonormal basis of  $\mathbf{V}_j$ . Let us denote by  $\mathbf{P}_{V_j}$  the orthogonal projection onto  $\mathbf{V}_j$ . Let  $f(x) \in \mathbf{L}^2(\mathbf{R})$ . The approximation of  $f(x)$  at the resolution  $2^j$  is the orthogonal projection of  $f(x)$  onto  $\mathbf{V}_j$  and thus given by

$$\mathbf{P}_{V_j} f(x) = \sum_{n=-\infty}^{+\infty} \langle f, \phi_{j,n} \rangle \phi_{j,n}(x), \quad (5)$$

where  $\langle , \rangle$  denotes the standard inner product in  $\mathbf{L}^2(\mathbf{R})$ . Since  $\mathbf{V}_{j-1} \subset \mathbf{V}_j$ , each space  $\mathbf{V}_j$  can be decomposed into

$$\mathbf{V}_j = \mathbf{V}_{j-1} \oplus \mathbf{W}_{j-1}, \quad (6)$$

where  $\mathbf{W}_{j-1}$  is the orthogonal complement of  $\mathbf{V}_{j-1}$  in  $\mathbf{V}_j$ . Let us denote by  $\mathbf{P}_{W_j}$  the orthogonal projection onto  $\mathbf{W}_j$ . From (6) we see that

$$\mathbf{P}_{V_j} f(x) = \mathbf{P}_{V_{j-1}} f(x) + \mathbf{P}_{W_{j-1}} f(x). \quad (7)$$

This relation indicates that an approximation at a resolution  $2^j$  can be decomposed into an approximation at a lower resolution  $2^{j-1}$  plus the “details” at the resolution  $2^j$  which are given by  $\mathbf{P}_{W_{j-1}}f(x)$ .

It can be shown [14],[12] that for any multiresolution approximation there exists a wavelet  $\psi(x)$  such that the family of functions  $(\psi_{j,n}(x))_{n \in \mathbb{Z}}$  is an orthonormal basis of  $\mathbf{W}_j$  at any resolution  $2^j$ . As a consequence of (6) and of property 3 of the multiresolution definition, we have that

$$\mathbf{L}^2(\mathbf{R}) = \bigoplus_{j=-\infty}^{+\infty} \mathbf{W}_j, \quad (8)$$

and all the spaces  $\mathbf{W}_j$  are mutually orthogonal. This implies that when the resolution index  $j$  varies from  $-\infty$  to  $+\infty$ , the family of functions  $(\psi_{j,n}(x))_{(n,j) \in \mathbb{Z}^2}$  is an orthonormal basis of  $\mathbf{L}^2(\mathbf{R})$ . Meyer [14] adapted multiresolution approximations and wavelet orthonormal bases of  $\mathbf{L}^2(\mathbf{R})$  to the space of functions in  $\mathbf{L}^2([0, 2^L])$  that are  $2^L$  periodic. We just need to periodize each function  $\psi_{j,n}$  with the summation

$$\tilde{\psi}_{j,n}(x) = \sum_{p=-\infty}^{+\infty} \psi_{j,n}(x - p2^L). \quad (9)$$

The resolution  $2^j$  must be larger than the inverse of the period, which is equal to  $2^{-L}$ , and the space  $\mathbf{V}_{-L}$  is the sub-space of functions in  $\mathbf{L}^2([0, 2^L])$  that are constant. One can show that the family  $(\tilde{\psi}_{j,n})_{j \geq -L, n \in \mathbb{Z}}$  is an orthogonal basis of the orthogonal complement of  $\mathbf{V}_{-L}$  in  $\mathbf{L}^2([0, 2^L])$ . These periodic wavelets are particularly useful for problems with periodic boundary conditions. Wavelets have also been adapted to deal with two-point boundary value problems by Xu and Shann [18].

In numerical computations, resolution is limited by memory constraints and computation times. Instead of working with a function  $f(x)$  we must consider its approximation up to a given resolution  $2^I$ :  $\mathbf{P}_{V_I}f(x)$ . This approximation can be decomposed into the detail spaces  $\mathbf{W}_j$  for  $j < I$ , up to some fixed coarser resolution  $2^J$ :

$$\mathbf{P}_{V_I}f(x) = \sum_{j=J}^{I-1} \mathbf{P}_{W_j}f(x) + \mathbf{P}_{V_J}f(x). \quad (10)$$

If we express these projections with an orthogonal basis for each space we obtain

$$\mathbf{P}_{V_I}f(x) = \sum_{j=J}^{I-1} \sum_{n=-\infty}^{+\infty} \langle f, \psi_{j,n} \rangle \psi_{j,n}(x) + \sum_{n=-\infty}^{+\infty} \langle f, \phi_{J,n} \rangle \phi_{J,n}(x) \quad (11)$$

Fig. 1 shows the grid of the wavelet coefficients corresponding to the decomposition of a function that belongs to  $\mathbf{V}_0$ . An orthogonal wavelet  $\psi(x)$  is generally centered around the abscissa  $x = \frac{1}{2}$ . Each wavelet function  $\psi_{j,n}(x)$  is thus centered around the point  $x = 2^{-j}n + 2^{-j-1}$  and the size of its support is proportional to  $2^{-j}$ . At a given resolution  $2^j$ , each cross corresponds to an inner product  $\langle f, \psi_{j,n} \rangle$ , called a wavelet coefficient. Its position corresponds to the center of the wavelet function  $\psi_{j,n}(x)$ . Each row of crosses corresponds to a layer of detail components that are needed to increase resolution from  $2^j$  to  $2^{j+1}$ . It corresponds to the projection  $\mathbf{P}_{W_j}f(x)$ . The array of crosses shown in Fig. 1 corresponds to the decomposition of a function that belongs to  $\mathbf{V}_0$ .

The absolute value of the wavelet coefficient  $|\langle f, \psi_{j,n} \rangle|$  depends upon the local regularity of  $f(x)$  in the neighborhood of the abscissa  $2^{-j}n$ . More precisely, if  $2^{-j}n \in ]a, b[$ , the decay of  $|\langle f, \psi_{j,n} \rangle|$  when the resolution  $2^j$  increases depends upon the Lipschitz regularity of  $f(x)$  over

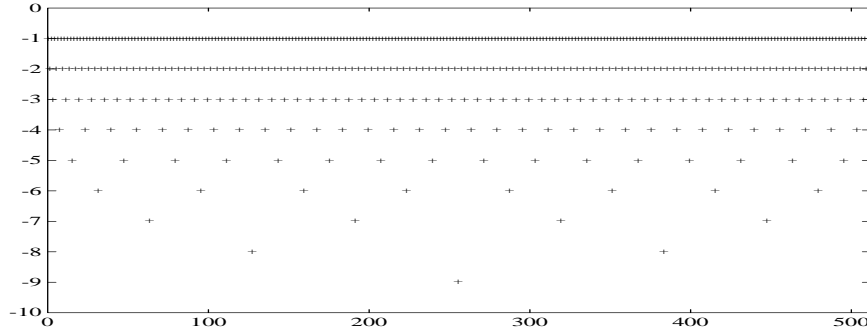


Figure 1: Grid of wavelet coefficients for a function that belongs to  $\mathbf{V}_0 = \mathbf{W}_{-1} \oplus \dots \oplus \mathbf{W}_{-9} \oplus \mathbf{V}_{-9}$ . Each cross represents a wavelet coefficient  $\langle f, \psi_{j,n} \rangle$  ( $n$  is along the  $x$ -axis and  $j$  the  $y$ -axis).

the interval  $]a, b[$ . Let us suppose that the wavelet  $\psi(x)$  is  $n$  times continuously differentiable and has  $n + 1$  vanishing moments:

$$\int_{-\infty}^{+\infty} x^p \psi(x) dx = 0 \quad \text{for } 0 \leq p \leq n. \quad (12)$$

**Theorem.** Let  $0 < \alpha < n$  be a real number that is not an integer. Let  $f(x) \in \mathbf{L}^2(\mathbb{R})$  and  $[a, b]$  be an interval. The function  $f(x)$  is uniformly Lipschitz of order  $\alpha$  over the interval  $[a, b]$  if and only if for any  $n \in \mathbb{Z}$  and  $j \in \mathbb{Z}$  such that  $2^{-j}n \in ]a, b[$ ,

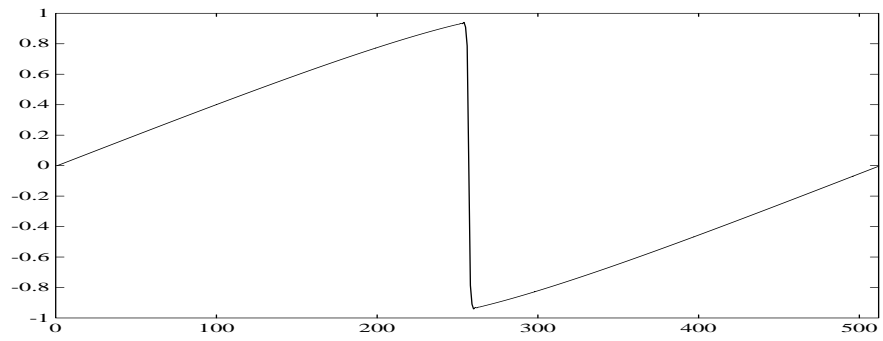
$$| \langle f, \psi_{j,n} \rangle | = O(2^{-(\alpha+1/2)j}). \quad (13)$$

The proof of this theorem can be found in Meyer's book [14]. It shows that the decay of the wavelet coefficients, as the resolution  $2^j$  increases, depends upon the local smoothness of the function. The larger the Lipschitz constant  $\alpha$ , the faster the decay of the wavelet coefficients. Fig. 2(a) shows a function that belongs to the space  $\mathbf{V}_0$  and has a sharp transition. Fig. 2(b) shows the grid of wavelet coefficients whose absolute value is larger than a given threshold. We see a pyramid of coefficients that points to the location of the sharp transition. The width of the pyramid depends on the size of the wavelet support. The number of wavelet coefficients at each resolution  $2^j$  is approximately a constant. Let us set to zero all the wavelet coefficients below some threshold. Out of 512 wavelet coefficients only 80 are non-zero. Let  $f_t(x)$  be the function reconstructed from these wavelet coefficients. Then

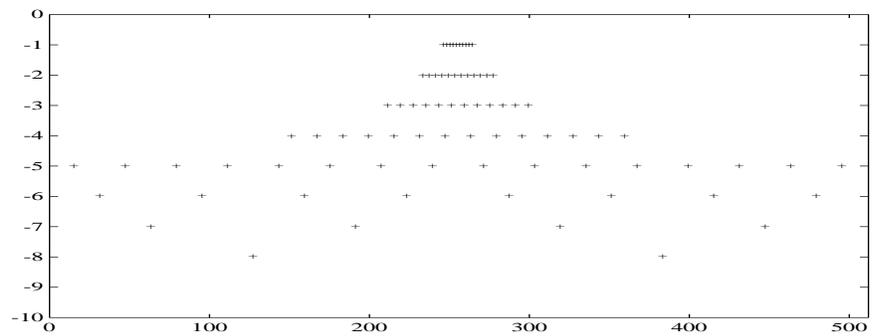
$$\frac{\|f - f_t\|_{\mathbf{L}^2(\mathbb{R})}}{\|f\|_{\mathbf{L}^2(\mathbb{R})}} = 8.6 \times 10^{-4}. \quad (14)$$

The function  $f_t(x)$  is a good approximation of  $f(x)$  because we removed only the wavelet coefficients of small amplitude. The pyramidal grid shown in Fig. 2(b) can be viewed as an adaptive grid where the resolution is adapted locally near the irregularity of the function. In the neighborhood of the abscissa 100 the function is very smooth and is thus locally approximated at the resolution  $2^{-5}$  whereas at the abscissa 256 the signal has a sharp transition and we need the full resolution. If the wavelet  $\psi(x)$  has  $n + 1$  vanishing moments, this pyramid of wavelet coefficients corresponds to a set of nested grids using finite elements of order  $n$ .

If the original function  $f(x)$  is given at a fixed resolution  $2^I$  by  $N$  values over a uniform grid, then all the wavelet coefficients  $\langle f, \psi_{j,n} \rangle$ , for  $j < I$  can be computed with a fast algorithm



(a)



(b)

Figure 2: (a) Function which belongs to  $\mathbf{V}_0$ . (b) Grid of wavelet coefficients for the function in Fig. 2(a). Only the wavelet coefficients larger than  $5 \times 10^{-3}$  are displayed. The analyzing wavelet is *spline 5*.

that requires  $O(N)$  operations [13]. A fast wavelet transform is thus faster than a fast Fourier transform. It is based on a cascade of convolutions with discrete filters called quadrature mirror filters [13]. The reconstruction of the original  $N$ -point function from the wavelet coefficients also requires  $O(N)$  operations. This fast wavelet transform algorithm is very effective in computationally intensive applications.

**Some examples of wavelet bases.** The properties of orthogonal wavelets derived from multiresolution approximations are now well understood [14],[13]. Different types of such wavelets can be constructed. The simplest possible wavelet is the Shannon wavelet whose Fourier transform is the indicator function

$$\hat{\psi}(\omega) = \begin{cases} 1 & \text{if } \pi \leq |\omega| \leq 2\pi \\ 0 & \text{otherwise} \end{cases} \quad (15)$$

This wavelet has compact support in the Fourier domain but has a slow decay in the spatial domain. Meyer showed that one can build wavelets which are infinitely differentiable and rapidly decreasing functions (Schwartz functions). These wavelets have also compact support in the Fourier domain while in the spatial domain their asymptotic decay at infinity is  $O(x^{-p})$  for any  $p > 0$ . For many applications the numerical decay of these wavelets is too slow. Battle [2] and Lemarie [10] have constructed polynomial spline wavelets with exponential decay that have good numerical properties. In the following, these wavelets are referred to as spline wavelets of order  $n$ , where  $n$  indicates that it is a polynomial spline of order  $n$ . Such a wavelet is  $n - 1$  times continuously differentiable, has  $n + 1$  vanishing moments and decays exponentially in the spatial domain. Daubechies [8] constructed orthogonal wavelets with compact support and an arbitrary degree of smoothness. We call such a compactly supported wavelet with  $n$  vanishing moments Daubechies  $n$ . Because of their compact support, the Daubechies wavelets are particularly useful in numerical applications.

### 3 Spatially adaptive wavelet methods for PDE's.

The ability of the wavelet transform to compress information by taking advantage of the local regularity of a function has many applications in signal processing and numerical analysis. Liandrat and Tchamitchian [11] as well as Perrier and Basdevant [16] have suggested that these properties should be used to do adaptive grid computations for PDE's. In this section, we describe the basic ideas of such adaptive schemes.

Suppose that we want to solve numerically an evolution equation

$$\begin{cases} \frac{\partial u(x, t)}{\partial t} = \mathbf{K}u(t, x) \\ u(0, x) = u_0(x) \end{cases} \quad (16)$$

where  $\mathbf{K}$  is an operator that acts on the  $x$  variable. The three examples that we study in detail are:

1. Diffusion equation:  $\mathbf{K}u(t, x) = \frac{\partial^2 u(t, x)}{\partial x^2}$ ,
2. Linear advection equation:  $\mathbf{K}u(t, x) = -\frac{\partial u(t, x)}{\partial x}$ ,
3. Burgers equation:  $\mathbf{K}u(t, x) = -u(t, x)\frac{\partial u(t, x)}{\partial x}$ .

For simplicity, we discretize time by a forward Euler scheme

$$\frac{\tilde{u}(t + \Delta t, x) - \tilde{u}(t, x)}{\Delta t} = \mathbf{K}\tilde{u}(t, x), \quad (17)$$

where  $\tilde{u}(t, x)$  is the approximate solution at time  $t$ . This leads to the explicit scheme

$$\tilde{u}(t + \Delta t, x) = (\mathbf{I} + \Delta t \mathbf{K})\tilde{u}(t, x). \quad (18)$$

This time discretization has poor stability properties for the linear advection and the Burgers equation. However, as explained later, we can use an explicit scheme of higher order in time that is stable for these equations. Let us for now suppose that (18) is stable.

The basic idea of a wavelet-based spatial adaptive scheme is to express equation (18) in a wavelet orthonormal basis. For each  $t$ , the function  $\tilde{u}(t, x)$  is represented by its wavelet coefficients. The operator  $\mathbf{I} + \Delta t \mathbf{K}$  is represented by a matrix in the same wavelet basis in order to compute directly the wavelet coefficients of  $\tilde{u}(t + \Delta t, x)$ .

Let us consider the matrix representation of a linear operator  $\mathbf{O}$  relative to a wavelet basis. We have

$$\mathbf{O} = \sum_{j=-\infty}^{+\infty} \sum_{l=-\infty}^{+\infty} \mathbf{P}_{W_l} \mathbf{O} \mathbf{P}_{W_j}. \quad (19)$$

Beylkin, Coifman and Roklin [6] have shown that if  $\mathbf{O}$  is a suitable pseudo-differential operator, each component  $\mathbf{P}_{W_l} \mathbf{O} \mathbf{P}_{W_j}$  can be approximated with arbitrarily high accuracy by a band matrix. This means that  $\mathbf{O}$  is represented by blocks of band matrices. In actual computations the infinite sums of (19) are finite. They are limited above by the finest resolution of the solution and below by the coarsest resolution  $2^J$ , as in equation (10). Fig. 3 shows how the operator  $\mathbf{O}$  acts on the wavelet coefficients of  $\tilde{u}(x, t)$ . In this example, the finest resolution  $2^I$  is equal to  $2^{-1}$  and the coarsest resolution  $2^J$  is equal to  $2^{-3}$ . The width of each band depends upon the properties of the operator  $\mathbf{O}$  and the size of the wavelet support.

If  $\mathbf{K}$  is a linear differential (or pseudo-differential) operator, then  $\mathbf{O} = \mathbf{I} + \Delta t \mathbf{K}$  is represented by band-matrices. If the solution  $\tilde{u}(t, x)$  has isolated sharp transitions, as in Fig. 2(a), we can set to zero its wavelet coefficients that are smaller than some threshold value, as in Fig. 2(b). Since  $\mathbf{O}$  is represented by blocks of band matrices, one can easily show that the domain where the wavelet coefficients of  $\tilde{u}(t + \Delta t, x)$  is non-negligible is at most equal to the corresponding domain for  $\tilde{u}(t, x)$  plus the width of the bands in the matrix that represents the operator  $\mathbf{O}$  in the wavelet basis (see Fig. 3). If  $P$  is the total number of nonzero wavelet coefficients of  $\tilde{u}(t, x)$ , the number of operations required to compute  $\mathbf{O}\tilde{u}(t, x)$  is  $O(P)$  [5]. For Burgers equation, the operator  $\mathbf{K}$  is nonlinear, so the previous result does not apply to  $\mathbf{O} = \mathbf{I} + \Delta t \mathbf{K}$ . However, Beylkin, Coifman and Roklin [6] have shown that the same computational complexity is obtained if  $\mathbf{O}$  is an n-linear operator. This is the case for Burgers equation since  $\mathbf{K}(u) = \partial_x u^2/2$  can be rewritten as  $\mathbf{K}(u) = \partial_x \mathbf{B}(u, u)/2$  where  $\mathbf{B}$  is the bilinear form  $\mathbf{B}(u, v) = uv$ . For the Burgers equation the number of operations required to compute  $(\mathbf{I} + \Delta t \mathbf{K})\tilde{u}(t, x)$  is still  $O(P)$ , where  $P$  is the number of nonzero wavelet coefficients of  $\tilde{u}(t, x)$ .

We see therefore how to take advantage of the compressed representation of  $\tilde{u}(t, x)$  in a wavelet basis in order to reduce the number of operations. Let us now describe the method suggested by Liandrat and Tchamitchian [11] as well as by Perrier and Basdevant [16] in order to adapt in time the spatial wavelet adaptive grid, and to follow singular structures of the solution. As we already explained, at each time  $t$  we keep the wavelet coefficients which are larger than a given threshold  $\lambda$ . In order to be able to track singularities we also keep the adjacent coefficients. We say that a wavelet coefficient  $\langle \tilde{u}, \psi_{j,n} \rangle$  is adjacent to another wavelet coefficient  $\langle \tilde{u}, \psi_{i,l} \rangle$  if and only if

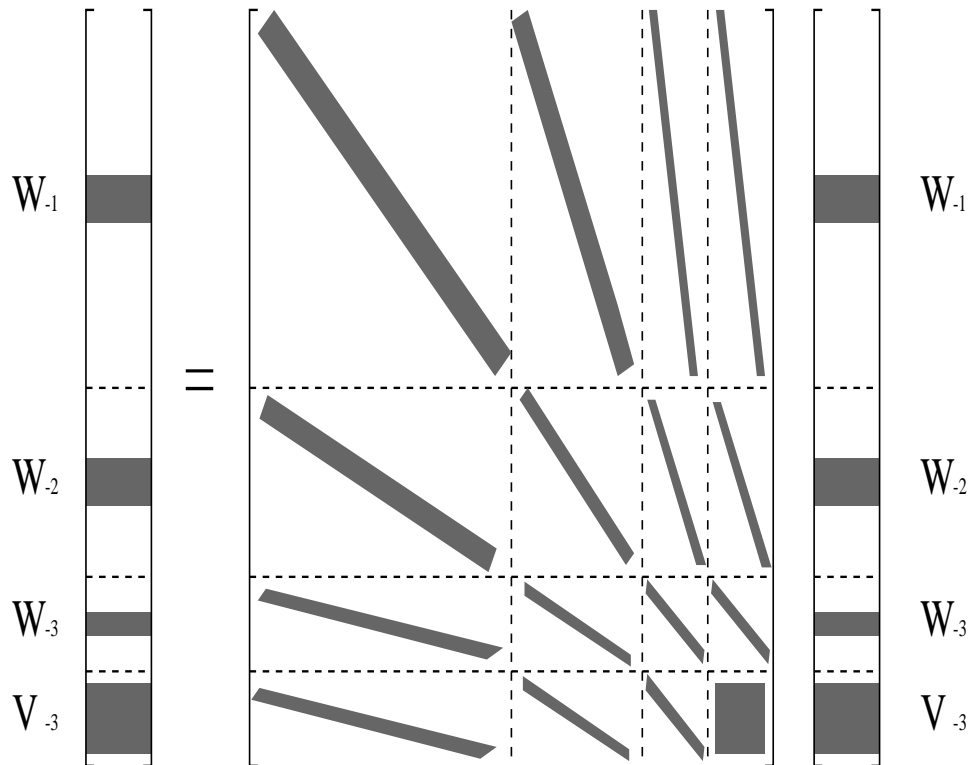


Figure 3: A pseudo-differential operator is represented by blocks of band matrices in a wavelet basis. When applied to a function that has few non-zero wavelet coefficients (shown by the grey area), the computational complexity is proportional to the number of non zero coefficients and the wavelet coefficients of the result are non zero in localized domains.

$i = j$  and  $|n - m| \leq 1$  or  $j = i + 1$  and  $l \leq n \leq l + 1$  (the apparent asymmetry of the last condition is due to the fact that a wavelet is centered at  $x = 1/2$  and not at  $x = 0$ ). In Fig. 4, the wavelet coefficients above the threshold  $\lambda$  are represented by crosses whereas the wavelet coefficients that are adjacent to the crosses (i.e., the “border” of the crosses set) are represented by circles. We denote by  $\mathcal{G}_t$  the grid of wavelet coefficients (crosses and circles) that are kept and represent the approximate solution at time  $t$ . The numerical algorithm is a 3 step loop:

1. In the previous step we have computed the wavelet coefficients of  $\tilde{u}(t, x)$  only at the positions of the grid  $\mathcal{G}_{t-\Delta t}$ ; the other coefficients are set to zero. We then adjust  $\mathcal{G}_{t-\Delta t}$  by changing into crosses the wavelet coefficients greater than the threshold and changing into circles their adjacent ones. This new set of circles and crosses defines the grid  $\mathcal{G}_t$ .
2. We project  $\tilde{u}(t, x)$  on the space corresponding to  $\mathcal{G}_t$ . This means that we put to zero all the wavelet coefficients of  $\tilde{u}(t, x)$  which do not correspond to crosses or circles of the new grid  $\mathcal{G}_t$ .
3. From equation (18) we compute the wavelet coefficients of  $\tilde{u}(t + \Delta t, x)$  corresponding to crosses and circles of the grid  $\mathcal{G}_t$ . We then go back to step 1.

The basic hypothesis behind this algorithm is that during a time  $\Delta t$ , the domain of crosses does not move in space and resolution beyond its border of circles. With such an algorithm the grid of wavelet coefficients is dynamically adapted in time and follows the local structures that appear in the solution.

The accuracy in the approximation of the adaptive grid of wavelet coefficients depends only upon the threshold coefficient  $\lambda$ . Fig. 4 shows the evolution of the wavelet grid for the solution of the periodic Burgers equation with initial condition  $u(0, x) = \sin(\pi x)$ . The solution is uniformly smooth initially and all the wavelet coefficients are below  $\lambda$  at resolutions larger than  $2^{-7}$ . The border of circles corresponds to the coefficients at the resolution  $2^{-6}$ . When the discontinuity develops some wavelet coefficients are no longer negligible at the resolution  $2^{-5}$  (and then part of the border of circles is at resolution  $2^{-4}$ ). In Figs 4(c) and 4(d), we see that the pyramid builds up progressively as the solution develops a sharper transition.

Wavelet orthonormal bases provide a simple procedure to implement spatial adaptive grids that are updated dynamically. We now concentrate on issues related to the discretization of the time parameter. In the next section we study first the heat equation and then the linear advection equation. In Section 5, we extend our results to Burgers equation.

## 4 Time Adaptive Resolution.

As we explained at the end of Section 1, in order to have a stable and accurate numerical scheme, the time discretization must be adapted to the spatial resolution of the computations. In this section, we explain how to introduce time adaptivity within the wavelet scheme described above. If we limit the computations to a resolution  $2^j$  then the time evolution equation

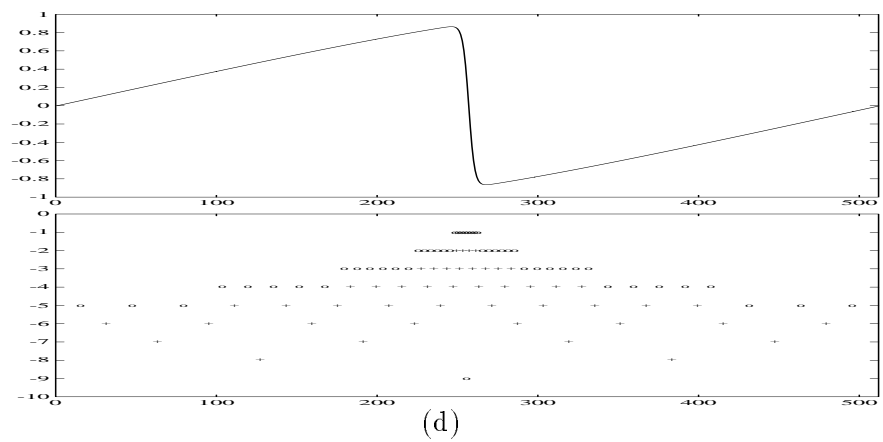
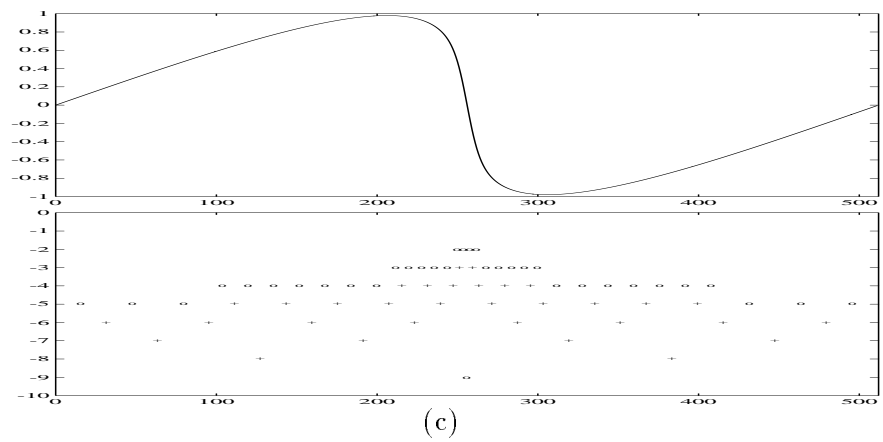
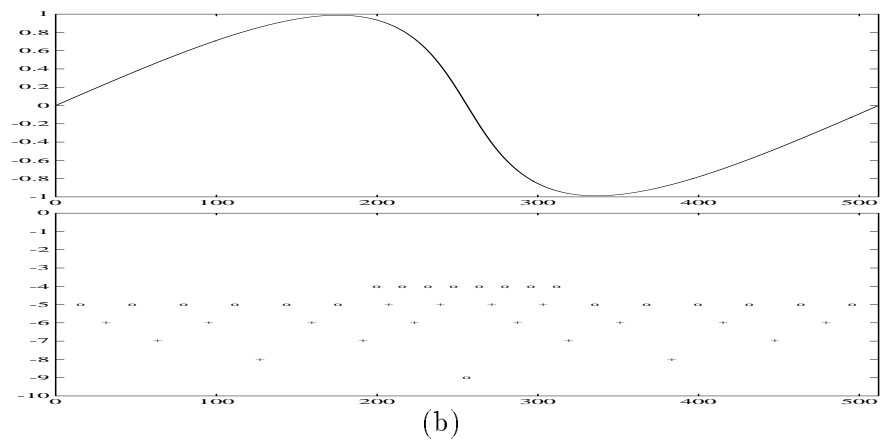
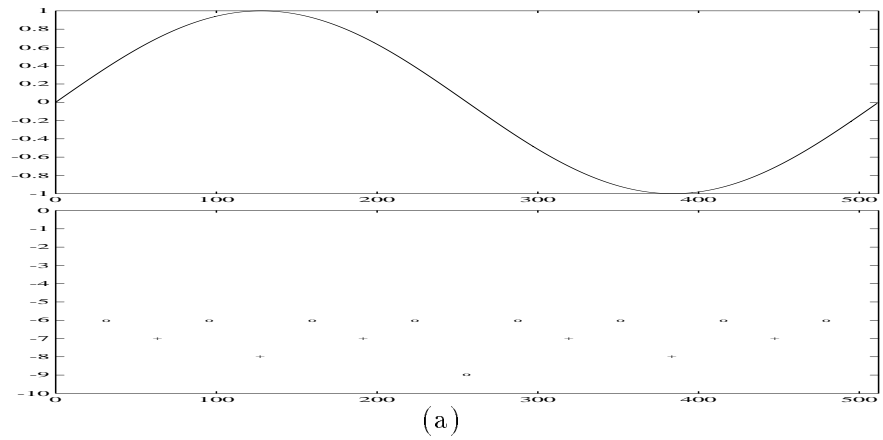
$$\frac{\partial u(x, t)}{\partial t} = \mathbf{K}u(t, x) \quad (20)$$

is replaced by

$$\frac{\partial u_j(x, t)}{\partial t} = \mathbf{K}_j u_j(t, x), \quad (21)$$

where the operator  $\mathbf{K}_j$  is defined by

$$\mathbf{K}_j = \mathbf{P}_{V_j} \mathbf{K} \mathbf{P}_{V_j}. \quad (22)$$



(the caption is at the top of the next page)

Figure 4: Evolution of the solution of the periodic Burgers equation. The initial condition  $u_0(x) = \sin(\pi x)$  is shown in (a). The grid of wavelet coefficients is displayed below each graph. Crosses indicate the wavelet coefficients larger than a given threshold and the circles are along the “borders” of the crosses.

The operator  $\mathbf{K}_j$  approximates the operator  $\mathbf{K}$  at the resolution  $2^j$  so that the solution  $u_j(t, x)$  remains in the space  $\mathbf{V}_j$ . The forward Euler discretization of (21) is

$$\tilde{u}_j(t + \Delta t, x) = (\mathbf{I} + \Delta t \mathbf{K}_j) \tilde{u}_j(t, x). \quad (23)$$

and it is stable if and only if

$$\|\mathbf{I} + \Delta t \mathbf{K}_j\| \leq 1. \quad (24)$$

As a first example, let us study the heat equation in some detail.

#### 4.1 Time Adaptivity for the Heat Equation.

For the heat equation

$$\mathbf{K} = \frac{\partial^2}{\partial x^2}.$$

Since  $\mathbf{K}$  is a nonpositive, symmetric operator,  $\mathbf{K}_j$  is also a nonpositive operator and thus equation (24) is equivalent to

$$\Delta t \|\mathbf{K}_j\| \leq 2. \quad (25)$$

We know that there exists a family of functions  $(\phi_{j,n}(x))_{n \in \mathbb{Z}}$ , with  $\phi_{j,n}(x) = \sqrt{2^j} \phi(2^j x - n)$ , which is an orthonormal basis of  $\mathbf{V}_j$ . By expressing the operator  $\mathbf{K}_j$  in this basis, we see that there exists a constant  $C$  such that

$$\|\mathbf{K}_j\| = C 2^{2j} = C 4^j. \quad (26)$$

Thus, the numerical scheme (23) is stable if and only if

$$\Delta t = \Delta t_j \leq \frac{2}{C} 4^{-j}. \quad (27)$$

When the spatial resolution is increased by a factor of 2, the upper bound of the time increment is divided by 4. To compute the solution with a resolution  $2^j$  at the time  $T = 1$  with a time step of  $\Delta t_j$ , the number of time steps is equal to  $1/\Delta t_j$ . Thus, to minimize the computations we must use a time step  $\Delta t_j$  that is as large as possible. The basic idea of the time adaptive algorithm is to modify the time step  $\Delta t_j$  at each resolution  $2^j$ .

Let us explain how to implement this idea by comparing the forward Euler scheme (23) at two successive resolutions  $2^I$  and  $2^{I-1}$ . At the resolution  $2^I$ , the solution  $\tilde{u}_I(t, x)$  belongs to  $\mathbf{V}_I$  and the Euler scheme is stable only if the time step  $\Delta t_I$  satisfies  $\Delta t_I \leq 2C^{-1} 4^{-I}$ . If we approximate the solution at the lower resolution  $2^{I-1}$ , the time step must satisfy  $\Delta t_{I-1} \leq 2C^{-1} 4^{-I+1}$  and so we may choose a time step four times larger,  $\Delta t_{I-1} = 4\Delta t_I$ . This is because the solution remains in the smaller space  $\mathbf{V}_{I-1}$ . We can decompose the higher resolution solution  $\tilde{u}_I(t, x)$  into its components in the spaces  $\mathbf{V}_{I-1}$  and  $\mathbf{W}_{I-1}$ . It is natural that the component in the space  $\mathbf{V}_{I-1}$  should be computed with a time step equal to  $\Delta t_{I-1}$  in a stable manner, while the component in  $\mathbf{W}_{I-1}$  should be computed with the smaller time step  $\Delta t_I$ .

Let us develop this idea further. At the resolution  $2^{I-1}$  the solution at time  $t + \Delta t_{I-1}$  is computed from the solution at time  $t$  by applying the operator  $\mathbf{I} + \Delta t_{I-1} \mathbf{K}_{I-1}$ :

$$\tilde{u}_{I-1}(t + \Delta t_{I-1}, x) = (\mathbf{I} + \Delta t_{I-1} \mathbf{K}_{I-1}) \tilde{u}_{I-1}(t, x). \quad (28)$$

At the resolution  $2^I$ ,  $\Delta t_I$  is four times smaller so we need 4 iterations to compute the solution at time  $t + \Delta t_{I-1}$ :

$$\tilde{u}_I(t + \Delta t_{I-1}, x) = \tilde{u}_I(t + 4\Delta t_I, x) = (\mathbf{I} + \Delta t_I \mathbf{K}_I)^4 \tilde{u}_I(t, x). \quad (29)$$

To relate equation (28) with equation (29), we decompose the operator  $\mathbf{K}_I$ . By definition

$$\mathbf{K}_I = \mathbf{P}_{V_I} \mathbf{K} \mathbf{P}_{V_I}. \quad (30)$$

Since  $\mathbf{P}_{V_I} = \mathbf{P}_{V_{I-1}} + \mathbf{P}_{W_{I-1}}$ , we obtain

$$\begin{aligned} \mathbf{K}_I &= \mathbf{P}_{V_{I-1}} \mathbf{K}_{I-1} \mathbf{P}_{V_{I-1}} + \mathbf{P}_{W_{I-1}} \mathbf{K}_{I-1} \mathbf{P}_{V_{I-1}} \\ &\quad + \mathbf{P}_{V_{I-1}} \mathbf{K}_{I-1} \mathbf{P}_{W_{I-1}} + \mathbf{P}_{W_{I-1}} \mathbf{K}_{I-1} \mathbf{P}_{W_{I-1}}. \end{aligned} \quad (31)$$

The operator  $\mathbf{K}_{I-1} = \mathbf{P}_{V_{I-1}} \mathbf{K} \mathbf{P}_{V_{I-1}}$  updates the components of lower resolution  $2^{I-1}$  to those of lower resolution  $2^{I-1}$ . The operator

$$\mathbf{T}_I = \mathbf{P}_{W_{I-1}} \mathbf{K}_{I-1} \mathbf{P}_{V_{I-1}} + \mathbf{P}_{V_{I-1}} \mathbf{K}_{I-1} \mathbf{P}_{W_{I-1}} + \mathbf{P}_{W_{I-1}} \mathbf{K}_{I-1} \mathbf{P}_{W_{I-1}} \quad (32)$$

updates the detail components on themselves and on those of lower resolution  $2^{I-1}$  as well as the low resolution components onto the detail components. Equation (31) implies that

$$\mathbf{K}_I = \mathbf{T}_I + \mathbf{K}_{I-1} \quad (33)$$

and using (33) in (29) we get

$$\tilde{u}_I(t + 4\Delta t_I, x) = (\mathbf{I} + \Delta t_I \mathbf{T}_I + \Delta t_I \mathbf{K}_{I-1})^4 \tilde{u}_I(t, x). \quad (34)$$

The scheme (28) suggests that the operator  $\mathbf{K}_{I-1}$  can be updated with a time step  $\Delta t_{I-1} = 4\Delta t_I$ , instead of  $\Delta t_I$ . We thus modify scheme (34) by updating  $\mathbf{K}_{I-1}$  with a time step  $4\Delta t_I$  while the  $\mathbf{T}_I$  component is updated with a time step  $\Delta t_I$

$$\tilde{u}_I(t + 4\Delta t_I, x) = \left( (\mathbf{I} + \Delta t_I \mathbf{T}_I)^4 + 4\Delta t_I \mathbf{K}_{I-1} \right) \tilde{u}_I(t, x). \quad (35)$$

In this scheme, the components at the lower resolution  $2^{I-1}$  are updated with a time step  $\Delta t_{I-1} = 4\Delta t_I$ , but the components of the higher resolution details are updated with a time step  $\Delta t_I$ . The numerical complexity to compute  $\mathbf{T}_I \tilde{u}_I(t, x)$  is proportional to the number of nonzero wavelet coefficients at the resolution  $2^I$ , whereas the complexity to compute  $\mathbf{K}_{I-1} \tilde{u}_I(t, x)$  is proportional to number of nonzero wavelet coefficients at all resolutions smaller than  $2^I$ . If the solution has isolated sharp transitions, as in Fig. 2, there are fewer wavelet coefficients at the resolution  $2^I$  than below this resolution (see Fig. 2(b)). Equation (35) thus requires substantially fewer computations than equation (34).

The same procedure can be repeated in order to adapt the time step to one more level of resolution. To compute the solution at  $t + 4^2 \Delta t_I$  we must iterate 4 times the operator previously defined

$$\tilde{u}_I(t + 4^2 \Delta t_I, x) = \left( (\mathbf{I} + \Delta t_I \mathbf{T}_I)^4 + 4\Delta t_I \mathbf{K}_{I-1} \right)^4 \tilde{u}_I(t, x). \quad (36)$$

Since we know that the operator  $\mathbf{K}_{I-2}$  by itself can be incremented by a time step  $\Delta t_{I-2} = 4^2 \Delta t_I$ , we decompose  $\mathbf{K}_{I-1}$  into

$$\mathbf{K}_{I-1} = \mathbf{T}_{I-1} + \mathbf{K}_{I-2} \quad (37)$$

as in (33). We then modify (36) as we did with (35) so that the time step is adapted to each component  $\mathbf{K}_{I-2}$  and  $\mathbf{T}_{I-1}$ . We obtain

$$\tilde{u}_I(t + 4^2 \Delta t_I, x) = \left( (\mathbf{I} + \Delta t_I \mathbf{T}_I)^4 + 4 \Delta t_I \mathbf{T}_{I-1} + 4^2 \Delta t_I \mathbf{K}_{I-2} \right) \tilde{u}_I(t, x). \quad (38)$$

This time adaptivity can now be applied on as many levels as desired. The general scheme can be formulated as follows. Let  $2^I$  be the finest resolution of computations,  $\Delta t_I$  be the time step at that resolution and let  $p$  be a positive integer. To compute the solution at a time  $t + 4^p \Delta t_I$  given the solution at time  $t$ , the forward Euler scheme based on the finest resolution gives

$$\tilde{u}_I(t + 4^p \Delta t_I, x) = (\mathbf{I} + \Delta t_I \mathbf{K}_I)^{4^p} \tilde{u}_I(t, x). \quad (39)$$

If the wavelet transform is computed over  $p$  ‘‘octaves’’ (i.e., on  $p$  resolutions), this can be rewritten in the form

$$\tilde{u}_I(t + 4^p \Delta t_I, x) = (\mathbf{I} + \Delta t_I \mathbf{T}_I + \Delta t_I \mathbf{T}_{I-1} + \dots + \Delta t_I \mathbf{T}_{I-p+1} + \Delta t_I \mathbf{K}_{I-p})^{4^p} \tilde{u}_I(t, x). \quad (40)$$

The time adaptive scheme replaces this scheme by

$$\tilde{u}_I(t + 4^p \Delta t_I, x) = \mathbf{E}_I^p \tilde{u}_I(t, x) \quad (41)$$

with

$$\mathbf{E}_I^p = (\dots((\mathbf{I} + \Delta t_I \mathbf{T}_I)^4 + 4 \Delta t_I \mathbf{T}_{I-1})^4 + \dots + 4^{p-1} \Delta t_I \mathbf{T}_{I-p+1})^4 + 4^p \Delta t_I \mathbf{K}_{I-p}. \quad (42)$$

In this scheme, (41) represents one iteration of the time adaptive operator  $\mathbf{E}_I^p$ . To compute the solution at a certain time  $T$  we must take  $T/(4^p \Delta t_I)$  steps with the operator  $\mathbf{E}_I^p$ . If  $p = 0$ , we obtain  $E_I^p = E_I^0 = (\mathbf{I} + \Delta t_I \mathbf{K}_I)^{T/\Delta t_I}$  which is the forward Euler scheme.

### Stability for the heat equation.

Let us now discuss the stability of this time adaptive scheme for the heat equation where  $\mathbf{K} = \partial^2/\partial x^2$ . From (27) we see that the forward Euler scheme (23) is stable at resolution  $2^I$ , if and only if

$$\Delta t_I \leq \frac{2}{C} 4^{-I}, \quad (43)$$

where the constant  $C$  is defined by (26) and the numerical scheme (41) is stable if and only if

$$\|\mathbf{E}_I^p\| \leq 1. \quad (44)$$

For the Shannon wavelet we prove in Appendix 1 that

$$\|\mathbf{E}_I^p\| \leq 1 \iff \Delta t_I \leq \frac{2}{C} 4^{-I}. \quad (45)$$

This means that the time adaptive scheme is stable for the same range of time steps  $\Delta t_I$  as the nonadaptive forward Euler scheme:

$$\|\mathbf{E}_I^p\| \leq 1 \iff \|\mathbf{I} + \Delta t_I \mathbf{K}_I\| \leq 1. \quad (46)$$

For the Shannon wavelet the proof of this result is simple because the operators  $\mathbf{T}_j$  are diagonal in a Fourier basis. For other wavelets we have no mathematical proof but numerical results seem to indicate that property (46) remains valid. We tested different wavelets that belong to the Meyer family [14], to the polynomial spline family of Battle [2] and Lemarie [10] and to the compactly supported family of Daubechies [8].

	<i>Forward Euler scheme</i>	<i>Time adaptive scheme</i>
<i>Shannon</i>	$9.987 \times 10^{-3}$	$9.987 \times 10^{-3}$
<i>Meyer</i>	$9.990 \times 10^{-3}$	$9.990 \times 10^{-3}$
<i>Spline 3</i>	$9.988 \times 10^{-3}$	$9.988 \times 10^{-3}$
<i>Spline 5</i>	$9.988 \times 10^{-3}$	$9.988 \times 10^{-3}$
<i>Spline 7</i>	$9.988 \times 10^{-3}$	$9.988 \times 10^{-3}$
<i>Spline 9</i>	$9.988 \times 10^{-3}$	$9.988 \times 10^{-3}$
<i>Daubechies 10</i>	$10.022 \times 10^{-3}$	$10.022 \times 10^{-3}$
<i>Daubechies 14</i>	$9.989 \times 10^{-3}$	$9.989 \times 10^{-3}$
<i>Daubechies 16</i>	$9.990 \times 10^{-3}$	$9.990 \times 10^{-3}$
<i>Daubechies 18</i>	$10.005 \times 10^{-3}$	$10.005 \times 10^{-3}$

Table 1: For each orthogonal wavelet listed in the first column, the second and third columns give the maximum time increment  $\Delta t_I$  for which the nonadaptive forward Euler scheme and the time adaptive scheme are stable, respectively. These values are equal which means that both schemes are stable over the same range of time increments.

We estimated numerically the stability of the scheme by computing the maximum  $\Delta t_I$  for which the  $\mathbf{L}^2(\mathbf{R})$  norm of the solution at any time  $t$  remains smaller than the norm of the initial condition  $u_0(x)$ . This means that the norm of the operator  $\mathbf{E}_I^p$  is smaller than 1. This test was done with an initial condition  $u_0(x)$  equal to the projection on  $\mathbf{V}_0$  of the indicator function of an interval, but the results are independent of the initial condition. To check the stability, we do not adapt the spatial resolution of the computations and thus do not apply a threshold to the wavelet coefficients. The initial solution is characterized by 64 wavelet coefficients and the time adaptive scheme is computed over 5 octaves, i.e.  $p = 5$  in equations (41) and (42). Table 1 gives the maximum time  $\Delta t_I$  for the nonadaptive in time forward Euler scheme and for the time adaptive scheme, with different wavelets. Since the resolution  $2^I$  is the same in these experiments, the maximum value of  $\Delta t_I$  varies with the constant  $C$  of equation (43), which depends upon the particular wavelet that is chosen. As expected from the proof in Appendix 1, for the Shannon wavelet the limit of stability is reached at the same maximum time increment  $\Delta t_I$  for the forward Euler scheme and for the time adaptive scheme. What is more interesting is that this result remains valid for all the other orthogonal wavelets that we checked. For the 10 different orthogonal bases given in Table 1, the maximum time step of the time adaptive scheme given in the last column is the same as the maximum time step of the nonadaptive in time scheme. We verified this property by computing the eigenvalues of the operators  $\mathbf{E}_I^p$  and  $\mathbf{I} + \Delta t_I \mathbf{K}_I$  and we checked that the maximum of their absolute value reaches 1 for the same time step  $\Delta t_I$ . It seems that this property is independent of the wavelet that is chosen and is a consequence of the multiresolution structure of wavelet orthonormal bases. We have no proof for this conjecture, which is motivated and supported by numerical results.

## 4.2 Time Adaptivity of the Linear Advection Equation.

Before considering Burgers equation, we introduce the space-time adaptive scheme for the linear advection equation,  $\mathbf{K} = -v\partial/\partial x$ , where  $v$  is the constant translation velocity. As in equation (21),

the PDE is approximated at the resolution  $2^j$  by

$$\frac{\partial u_j(x, t)}{\partial t} = \mathbf{K}_j u_j(t, x), \quad (47)$$

where the operator  $\mathbf{K}_j$  is defined by

$$\mathbf{K}_j = \mathbf{P}_{V_j} \mathbf{K} \mathbf{P}_{V_j}. \quad (48)$$

One can easily prove that

$$\|\mathbf{K}_j\| = C 2^j. \quad (49)$$

The explicit forward Euler scheme is unstable for a linear advection, so we use instead the explicit Adams-Bashforth scheme which is defined by

$$\tilde{u}_j(t + \Delta t_j, x) = \tilde{u}_j(t, x) + \Delta t_j (a \mathbf{K}_j \tilde{u}_j(t, x) + b \mathbf{K}_j \tilde{u}_j(t - \Delta t_j, x) + c \mathbf{K}_j \tilde{u}_j(t - 2\Delta t_j, x)), \quad (50)$$

with  $a = 33/12$ ,  $b = -16/12$ ,  $c = 5/12$ . Stability results from using the past values of  $\tilde{u}_j(t, x)$  at time  $t - \Delta t_j$  and  $t - 2\Delta t_j$ . We denote by  $\|\tilde{u}_j(t, x)\|$  the  $\mathbf{L}^2(\mathbf{R})$  norm of  $\tilde{u}_j(t, x)$  in the  $x$  variable. One can prove that this scheme is stable in the sense that

$$\|\tilde{u}_j(t + \Delta t_j, x)\| \leq \text{Max} (\|\tilde{u}_j(t, x)\|, \|\tilde{u}_j(t - \Delta t_j, x)\|, \|\tilde{u}_j(t - 2\Delta t_j, x)\|)$$

at any time  $t$  and for any initial condition, if and only if

$$\Delta t_j \leq C' 2^{-j}. \quad (51)$$

The constant  $C'$  depends only upon the constant  $C$  defined by equation (49). This simple definition of stability enables us to compare more easily the stability of the time adaptive scheme versus the nonadaptive in time scheme. From the initial condition  $\tilde{u}_j(0, x) = u_0(x)$ , we compute the first two steps  $\tilde{u}_j(\Delta t_j, x)$  and  $\tilde{u}_j(2\Delta t_j, x)$  with a forward Euler scheme. If the initial condition  $u_0(x)$  is four times continuously differentiable, the error introduced by the time discretization when computing the solution at  $T = 1$  is  $O(\Delta t_j^2)$ .

The Adams-Bashforth scheme (50) can be rewritten in matrix form. Let us define

$$U_j(t, x) = \begin{pmatrix} \tilde{u}_j(t, x) \\ \tilde{u}_j(t - \Delta t_j, x) \\ \tilde{u}_j(t - 2\Delta t_j, x) \end{pmatrix} \quad (52)$$

and the following matrix of operators

$$\mathbf{K}_j U_j(t, x) = \begin{pmatrix} a \mathbf{K}_j \tilde{u}_j(t, x) + b \mathbf{K}_j \tilde{u}_j(t - \Delta t_j, x) + c \mathbf{K}_j \tilde{u}_j(t - 2\Delta t_j, x) \\ 0 \\ 0 \end{pmatrix}, \quad (53)$$

$$\mathbf{I} U_j(t, x) = \begin{pmatrix} \tilde{u}_j(t, x) \\ \tilde{u}_j(t, x) \\ 0 \end{pmatrix}, \quad (54)$$

$$\mathbf{M}_j U_j(t, x) = \begin{pmatrix} 0 \\ 0 \\ \tilde{u}_j(t - \Delta t_j, x) \end{pmatrix}. \quad (55)$$

The operator  $\mathbf{I}$  plays the role of the identity, as in a forward Euler scheme (23), but it also updates the first memory component. The memory component at time  $t - \Delta t_j$  is updated by the operator  $\mathbf{M}_j$ . The Adams-Bashforth equation (50) takes the form

$$U_j(t + \Delta t_j, x) = (\mathbf{I} + \Delta t_j \mathbf{K}_j + \mathbf{M}_j) U_j(t, x). \quad (56)$$

It has the same structure as the explicit Euler scheme (23) but includes a “memory” component which is carried by the operator  $\mathbf{M}_j$ . To obtain a time adaptive scheme we proceed as we did with the heat equation except for two important differences:

1. The stability condition (51) implies that the time step can increase by a factor 2 and not 4 when the resolution decreases from  $2^I$  to  $2^{I-1}$ :  $\Delta t_{I-1} = 2\Delta t_I$ .
2. We must also have a time adaptive memory component.

To introduce the time adaptive scheme, as in subsection 4.1, we compare the Adams-Bashforth scheme at the resolutions  $2^I$  and  $2^{I-1}$ . At the resolution  $2^I$  and for a time step  $\Delta t_I$ , the Adams-Bashforth scheme requires the storage of  $\tilde{u}_I(t, x)$ ,  $\tilde{u}_I(t - \Delta t_I, x)$  and  $\tilde{u}_I(t - 2\Delta t_I, x)$ . At the resolution  $2^{I-1}$  and for a time step  $\Delta t_{I-1} = 2\Delta t_I$ , it requires to keep the solution at  $t$ ,  $t - 2\Delta t_I$  and  $t - 2^2\Delta t_I$ . To make the two schemes comparable, we must therefore use a memory vector that has four components

$$U_I^1(t, x) = \begin{pmatrix} \tilde{u}_I(t, x) \\ \tilde{u}_I(t - \Delta t_I, x) \\ \tilde{u}_I(t - 2\Delta t_I, x) \\ \tilde{u}_I(t - 2^2\Delta t_I, x) \end{pmatrix}. \quad (57)$$

Let us recall that the component of the operator  $\mathbf{K}$  related to the projection of the solution on the space  $\mathbf{W}_{I-1}$  is defined

$$\mathbf{T}_I = \mathbf{K}_I - \mathbf{K}_{I-1}, \quad (58)$$

and can also be written as in (32). We define the operator  $\mathbf{T}_I^1$  by

$$\mathbf{T}_I^1 U_I^1(t, x) = \begin{pmatrix} a\mathbf{T}_I \tilde{u}_I(t, x) + b\mathbf{T}_I \tilde{u}_I(t - \Delta t_I, x) + c\mathbf{T}_I \tilde{u}_I(t - 2\Delta t_I, x) \\ 0 \\ 0 \\ 0 \end{pmatrix}, \quad (59)$$

It uses the first three components of  $U_I^1$  to compute the part of  $\tilde{u}_I(t + \Delta t_I, x)$  which is related to the  $\mathbf{W}_{I-1}$  space. At the resolution  $2^{I-1}$ , the Adams-Bashforth scheme is computed with the operator  $\mathbf{K}_{I-1}^1$ :

$$\mathbf{K}_{I-1}^1 U_I^1(t, x) = \begin{pmatrix} a\mathbf{K}_{I-1} \tilde{u}_I(t, x) + b\mathbf{K}_{I-1} \tilde{u}_{I-1}(t - 2\Delta t_I, x) + c\mathbf{K}_{I-1} \tilde{u}_{I-1}(t - 2^2\Delta t_I, x) \\ 0 \\ 0 \\ 0 \end{pmatrix}. \quad (60)$$

Then, the operator  $\mathbf{I}$  defined in (53) becomes

$$\mathbf{I}^1 U_I^1(t, x) = \begin{pmatrix} \tilde{u}_I(t, x) \\ \tilde{u}_I(t, x) \\ 0 \\ 0 \end{pmatrix}. \quad (61)$$

The updates of the memory components at the resolutions  $2^I$  and  $2^{I-1}$  are respectively given by

$$\mathbf{M}_I^1 U_I^1(t, x) = \begin{pmatrix} 0 \\ 0 \\ \tilde{u}_I(t - \Delta t_I, x) \\ 0 \end{pmatrix} \quad (62)$$

$$\mathbf{M}_{I-1}^1 U_I^1(t, x) = \begin{pmatrix} 0 \\ 0 \\ 0 \\ \tilde{u}_I(t - 2\Delta t_I, x) \end{pmatrix}. \quad (63)$$

As in the heat equation (35), we obtain a time adaptive Adams-Bashforth scheme by updating the higher resolution component twice as fast as the lower resolution one:

$$U_I^1(t + 2\Delta t_I, x) = \left( (\mathbf{I}^1 + \Delta t_I \mathbf{T}_I^1 + \mathbf{M}_I^1)^2 + 2\Delta t_I \mathbf{K}_{I-1}^1 + \mathbf{M}_{I-1}^1 \right) U_I^1(t, x). \quad (64)$$

The memory component at the resolution  $2^I$  is updated by the operator  $\mathbf{M}_I^1$  whereas  $\mathbf{M}_{I-1}^1$  updates the memory component at the resolution  $2^{I-1}$ .

Let us now introduce the general time adaptive scheme. Let  $2^I$  be the finest resolution of the computation. Let  $p$  be a positive integer and we suppose that the wavelet transform is computed over  $p$  octaves. The time adaptive scheme requires a memory vector with  $p + 3$  components:

$$U_I^p(t, x) = \begin{pmatrix} \tilde{u}_I(t, x) \\ \tilde{u}_I(t - \Delta t_I, x) \\ \tilde{u}_I(t - 2\Delta t_I, x) \\ \vdots \\ \tilde{u}_I(t - 2^{p+1}\Delta t_I, x) \end{pmatrix}. \quad (65)$$

In the same way as above, the identity plus the update of the first memory component is given by

$$\mathbf{I}^p U_I^p(t, x) = \begin{pmatrix} \tilde{u}_I(t, x) \\ \tilde{u}_I(t, x) \\ 0 \\ \vdots \\ 0 \end{pmatrix}. \quad (66)$$

For any resolution  $2^{I-k}$ , with  $k < p$ , we define the operator

$$\mathbf{T}_{I-k}^p U_I^p(t, x) = \begin{pmatrix} a\mathbf{T}_{I-k}\tilde{u}_I(t, x) + b\mathbf{T}_{I-k}\tilde{u}_I(t - 2^k\Delta t_I, x) + c\mathbf{T}_{I-k}\tilde{u}_I(t - 2^{k+1}\Delta t_I, x) \\ 0 \\ \vdots \\ 0 \end{pmatrix}. \quad (67)$$

At the same resolution  $2^{I-k}$ , the memory component is updated by the operator

$$\mathbf{M}_{I-k}^p U_I^p(t, x) = \begin{pmatrix} 0 \\ \vdots \\ 0 \\ \tilde{u}_I(t - 2^k\Delta t_I, x) \\ 0 \\ \vdots \\ 0 \end{pmatrix}, \quad (68)$$

whose only non-zero element is the  $(k+3)^d$  one. At the lowest resolution  $2^{I-p}$ , we use the operator

$$\mathbf{K}_{I-p}^p U_I^p(t, x) = \begin{pmatrix} a\mathbf{K}_{I-p}\tilde{u}_I(t, x) + b\mathbf{K}_{I-p}\tilde{u}_I(t - 2^p\Delta t_I, x) + c\mathbf{K}_{I-p}\tilde{u}_I(t - 2^{p+1}\Delta t_I, x) \\ 0 \\ \vdots \\ 0 \end{pmatrix}. \quad (69)$$

At each resolution the time adaptive scheme is then defined naturally, as in (41), by

$$U_I^p(t + 2^p\Delta t_I, x) = \mathbf{E}_I^p U_I^p(t, x) \quad (70)$$

with

$$\begin{aligned} \mathbf{E}_I^p = & \left( \dots \left( (\mathbf{I} + \Delta t_I \mathbf{T}_I^p + \mathbf{M}_I^p)^2 + 2\Delta t_I \mathbf{T}_{I-1}^p + \mathbf{M}_{I-1}^p \right)^2 + \dots \right. \\ & \left. \dots + 2^{p-1}\Delta t_I \mathbf{T}_{I-p-1}^p + \mathbf{M}_{I-p-1}^p \right)^2 + 2^p\Delta t_I \mathbf{K}_{I-p}^p + \mathbf{M}_{I-p}^p. \end{aligned} \quad (71)$$

Let us note that in order to compute the solution at time  $T$  we need to apply this operator  $T/(2^p\Delta t_I)$  times. From the initial condition at  $t = 0$  we can compute each component of the initial memory vector  $U_I^p(2^{p+1}\Delta t_I, x)$  with an explicit forward Euler scheme.

### Stability for the advection equation.

Let us now discuss the stability of this time adaptive scheme. We say that the scheme is stable if and only if at any time  $t$  and for any initial condition  $U_I^p(0, x)$ , all the components of the vector  $U_I^p(t, x)$  have an  $\mathbf{L}^2(\mathbf{R})$  norm in the  $x$  variable, which is smaller than or equal to the maximum  $\mathbf{L}^2(\mathbf{R})$  norm of the components of the initial condition  $U_I^p(0, x)$ . We mentioned in (51) that the Adams-Bashforth scheme for the advection equation (50) is stable if and only if

$$\Delta t_I \leq C'2^{-I}. \quad (72)$$

For the Shannon wavelet (15), we show in Appendix 2 that the numerical scheme defined by  $\mathbf{E}_I^p$  remains stable over the same range of time steps  $\Delta t_I$  as the nonadaptive in time scheme (50). For this wavelet, the proof is relatively simple because all the operators involved are diagonalized by the Fourier transform. As in the case of the heat equation, for other wavelets we test for the stability of the time adaptive and nonadaptive in time schemes by computing the maximum time increments for which they remain stable. In these experiments we do not apply a threshold to the wavelet coefficients which means that we do not introduce any spatial adaptivity.

This test was done with an initial condition  $u_0(x)$  equal to the projection on  $\mathbf{V}_0$  of the indicator function of an interval. The initial solution is characterized by 64 wavelet coefficients and the time adaptive scheme is computed over 5 octaves, i.e.  $p = 5$  in equations (70) and (71). Table 2 gives the maximum time  $\Delta t_I$  for which the nonadaptive Adams-Bashforth and the time adaptive schemes remain stable. This maximum time step is computed with less accuracy than for the heat equation because of the necessity to compute the first few steps directly, given the initial condition at  $t = 0$ . As expected from the proof in Appendix 2, when the accuracy of the computation is fixed, the limit of stability for the Shannon wavelet is reached at the same maximum time increment  $\Delta t_I$  for both the Adams-Bashforth and the time adaptive scheme. For the Meyer wavelet as well as for the spline wavelets of Battle [2] and Lemarie [10], the maximum time step is the same for the time adaptive and the nonadaptive in time schemes, with the accuracy of our numerical computations fixed. On the other hand, this result is not valid for the Daubechies wavelets, although the values of

	<i>Adams Bashforth scheme</i>	<i>Time adaptive scheme</i>
<i>Shannon</i>	$3.61 \times 10^{-3}$	$3.61 \times 10^{-3}$
<i>Meyer</i>	$5.25 \times 10^{-3}$	$5.25 \times 10^{-3}$
<i>Spline 3</i>	$4.99 \times 10^{-3}$	$4.99 \times 10^{-3}$
<i>Spline 5</i>	$4.52 \times 10^{-3}$	$4.52 \times 10^{-3}$
<i>Spline 7</i>	$4.30 \times 10^{-3}$	$4.30 \times 10^{-3}$
<i>Spline 9</i>	$4.19 \times 10^{-3}$	$4.19 \times 10^{-3}$
<i>Daubechies 10</i>	$6.27 \times 10^{-3}$	$5.48 \times 10^{-3}$
<i>Daubechies 14</i>	$5.78 \times 10^{-3}$	$5.39 \times 10^{-3}$
<i>Daubechies 16</i>	$5.44 \times 10^{-3}$	$5.21 \times 10^{-3}$
<i>Daubechies 18</i>	$5.48 \times 10^{-3}$	$5.37 \times 10^{-3}$

Table 2: For each orthogonal wavelet listed in the first column, the second and third columns give the maximum time increment  $\Delta t_I$  for which the Adams-Bashforth scheme and the time adaptive scheme are stable, respectively.

the maximum time steps remain close. We do not know why the stability of the scheme is different for the Daubechies wavelets. The Daubechies wavelets have compact support and they are neither symmetric nor antisymmetric in contrast to the wavelets of Meyer and Battle-Lemarie. We note that when the support of the Daubechies wavelet increases, the difference between the maximum time step of both schemes decreases but it is not clear why this is happening. We emphasize, however, that even in the Daubechies case, the schemes are stable over a comparable range of time increments.

### Complexity estimates for the advection equation.

Let us now discuss the numerical complexity of the time and space adaptive scheme as compared to the space adaptive scheme that is not time adaptive. Since the linear advection equation just translates the initial solution, the number of non-negligible wavelet coefficients remains approximately constant in time. Let  $2^I$  be the finest resolution and suppose that the wavelet transform is computed over  $p$  octaves. The solution is decomposed onto  $\mathbf{V}_I = \bigoplus_{j=I-p+1}^I \mathbf{W}_{j-1} \oplus \mathbf{V}_{I-p}$ . We denote by  $N$  the number of wavelet coefficients that characterize the projection of the solution in  $V_I$  (number of samples). The projection of the solution on  $\mathbf{V}_{I-p}$  is characterized by  $2^{-p}N$  coefficients. Let  $n_j$  ( $j < I$ ) be the number of nonzero wavelet coefficients (after applying a threshold) that characterize the projection of the solution on  $\mathbf{W}_{j-1}$ . The total number of nonzero coefficients in the grid is then equal to  $\sum_{j=I-p+1}^I n_j + 2^{-p}N$ . We thus see that the nonadaptive in time scheme (50) requires

$$O \left( \sum_{j=I-p+1}^I n_j + 2^{-p}N \right) \quad (73)$$

operations per time step. The constant depends mostly on the size of the wavelet support. To compute the solution at time  $T = 1$ , we need  $1/\Delta t_I$  time steps and the total number of operations

is

$$O\left(\frac{1}{\Delta t_I}\left(\sum_{j=I-p+1}^I n_j + 2^{-p}N\right)\right). \quad (74)$$

For the time adaptive scheme (70), the complexity of computing the action of each operator  $\mathbb{T}_j$  on the solution is also  $O(n_j)$ . The time step associated to the operator  $\mathbb{T}_j$  is  $\Delta t_j = 2^{I-j}\Delta t_I$ . The total complexity of the scheme to compute the solution at  $T = 1$  is therefore

$$O\left(\frac{1}{\Delta t_I}\left(\sum_{j=I-p+1}^I 2^{j-I}n_j + 2^{-p}2^{-p}N\right)\right). \quad (75)$$

The constants in (74) and (75) are approximately the same and depend on the size of the wavelet support. If the solution has fine structures over its whole support, then there are almost no negligible wavelet coefficients and  $n_j \simeq N2^{j-I-1}$ . The complexity given by both (74) and (75) is

$$O\left(\frac{N}{\Delta t_I}\right). \quad (76)$$

We therefore realize no gain with a time adaptive scheme. This is not surprising since half of the wavelet coefficients are at the largest resolution  $2^I$  and the time step at this resolution is the same for both the time adaptive and the nonadaptive in time schemes. The time adaptive scheme is efficient only if the spatial adaptive grid has already removed many wavelet coefficients. This is the case when the solution has only isolated singularities. If we suppose that the initial solution has isolated sharp variations, as in Fig. 2(a), then the nonzero wavelet coefficients belong to pyramids similar to Fig. 2(b). Each pyramid corresponds to a particular singularity. At each resolution level, the number of nonzero wavelet coefficients  $n_k$  is approximately equal to a constant  $L$ , which depends upon the size of the wavelet support. The complexity of the nonadaptive in time scheme given by (50) becomes

$$O\left(\frac{1}{\Delta t_I}(pL + 2^{-p}N)\right), \quad (77)$$

whereas the complexity of the time-adaptive scheme is

$$O\left(\frac{1}{\Delta t_I}(L + 2^{-p}2^{-p}N)\right). \quad (78)$$

If the support of the signal is very large, and the number of wavelet coefficients  $L$  at each resolution is negligible with respect to the remaining coefficients  $2^{-p}N$ , then the gain of the time adaptive scheme is a factor of  $2^p$ . Otherwise ( $2^{-p}N \simeq L$ ), the gain is proportional to the number of octaves  $p$  of the wavelet decomposition. Since  $p$  is generally of the order of  $\log_2(N)$ , the complexity gain is approximately  $\log_2(N)$ . Let us emphasize here that the constants in the complexity estimates (77) and (78) are the same so that the gain is not lost by the size of the constant factors. On the other hand, since we use larger time steps at coarser resolutions, it is likely that we also increase the numerical errors of the scheme. The accuracy of the time-adaptive scheme is studied in the more interesting case of Burgers equation.

## 5 Burgers Equation.

In this section, we compare the stability, accuracy and numerical complexity of the wavelet based space and time adaptive scheme with a wavelet based scheme which is space adaptive but not

time adaptive. We do not compare our algorithm with more classical numerical schemes, such as spectral methods or finite elements, because this type of comparison has been done by Liandrat and Tchamitchian [11] for the space adaptive wavelet scheme. With Burgers equation we want to study specifically the impact of the time adaptivity on the computed solution.

### 5.1 Time Adaptive Algorithm.

The periodic Burgers equation with small diffusion is given by

$$\frac{\partial u(x, t)}{\partial t} = \mathbf{K}u(t, x), \quad (79)$$

where  $\mathbf{K}$  is the nonlinear operator

$$\mathbf{K}u(t, x) = -u(t, x)\frac{\partial u(t, x)}{\partial x} + \epsilon\frac{\partial^2 u(t, x)}{\partial x^2}, \quad (80)$$

and the initial solution  $u(x, 0) = u_0(x)$  is periodic with period 1. For the time discretization, we use an explicit Adams-Bashforth scheme for the advection term and an explicit Euler scheme for the diffusion. The time adaptive scheme we have implemented for the advection term is essentially the same as the one describe in Section 4. At each resolution  $2^j$  the time step is  $\Delta t_j = 2^{I-j}\Delta t_I$ . In order for the diffusion term to remain in step with the time adaptivity of the advection term, we use the time increment  $2^{I-j}\Delta t_I$  instead of  $4^{I-j}\Delta t_I$ , at a resolution  $2^j$ .

Let us separate the advection and the diffusion terms and define the two operators

$$\mathbf{K}^0 f(x) = -f(x)\frac{\partial f(x)}{\partial x} \quad (81)$$

and

$$\mathbf{K}^1 f(x) = \epsilon\frac{\partial^2 f(x)}{\partial x^2}. \quad (82)$$

Let  $\mathbf{K}_j^0 = \mathbf{P}_{V_j}\mathbf{K}^0\mathbf{P}_{V_j}$  and  $\mathbf{K}_j^1 = \mathbf{P}_{V_j}\mathbf{K}^1\mathbf{P}_{V_j}$ . We also define  $\mathbf{T}_j^0 = \mathbf{K}_j^0 - \mathbf{K}_{j-1}^0$  and  $\mathbf{T}_j^1 = \mathbf{K}_j^1 - \mathbf{K}_{j-1}^1$ . An explicit forward Euler scheme is sufficient for the diffusion term  $\mathbf{K}^0$ , whereas the nonlinear advection operator  $\mathbf{K}^1$  requires an Adams-Bashforth scheme. Both components are integrated in a time-adaptive scheme which is similar to the linear advection, time adaptive scheme. Let  $2^I$  be the finest resolution of computation. Let  $p$  be a positive integer and we suppose that the wavelet transform is computed over  $p$  octaves. The advection operator  $\mathbf{K} = -\partial/\partial x$  is replaced by  $\mathbf{K}^0$  and we manage the memory component in the same way as in (71). The diffusion term  $\mathbf{K}^1$  does not use any memory component. As in the linear advection scheme, the memory vector is defined by

$$U_I^p(t, x) = \begin{pmatrix} \tilde{u}_I(t, x) \\ \tilde{u}_I(t - \Delta t_I, x) \\ \tilde{u}_I(t - 2\Delta t_I, x) \\ \vdots \\ \tilde{u}_I(t - 2^{p+1}\Delta t_I, x) \end{pmatrix}. \quad (83)$$

The operators are given by

$$\mathbf{I}^p U_I^p(t, x) = \begin{pmatrix} \tilde{u}_I(t, x) \\ \tilde{u}_I(t, x) \\ 0 \\ \vdots \\ 0 \end{pmatrix}, \quad (84)$$

$$\mathbf{T}_{I-k}^p U_I^p(t, x) = \begin{pmatrix} a\mathbf{T}_{I-k}^0 \tilde{u}_I(t, x) + b\mathbf{T}_{I-k}^0 \tilde{u}_I(t - 2^k \Delta t_I, x) + c\mathbf{T}_{I-k}^0 \tilde{u}_I(t - 2^{k+1} \Delta t_I, x) \\ \quad + \mathbf{T}_{I-k}^1 \tilde{u}_I(t, x) \\ 0 \\ \vdots \\ 0 \end{pmatrix} \quad (85)$$

$$\mathbf{M}_{I-k}^p U_I^p(t, x) = \begin{pmatrix} 0 \\ \vdots \\ 0 \\ \tilde{u}_I(t - 2^k \Delta t_I, x) \\ 0 \\ \vdots \\ 0 \end{pmatrix} \quad (86)$$

where the only non zero coefficient is the  $(k + 3)^d$  one, and

$$\mathbf{K}_{I-p}^p U_I^p(t, x) = \begin{pmatrix} a\mathbf{K}_{I-p}^0 \tilde{u}_I(t, x) + b\mathbf{K}_{I-p}^0 \tilde{u}_I(t - 2^p \Delta t_I, x) + c\mathbf{K}_{I-p}^0 \tilde{u}_I(t - 2^{p+1} \Delta t_I, x) \\ \quad + \mathbf{K}_{I-p}^1 \tilde{u}_I(t, x) \\ 0 \\ \vdots \\ 0 \end{pmatrix}. \quad (87)$$

The Burgers time adaptive scheme is then defined by

$$U_I^p(t + 4^p \Delta t_I, x) = \mathbf{E}_I^p U_I^p(t, x) \quad (88)$$

with

$$\mathbf{E}_I^p = \left( \dots \left( (\mathbf{I} + \Delta t_I \mathbf{T}_I^p + \mathbf{M}_I^p)^2 + 2\Delta t_I \mathbf{T}_{I-1}^p + \mathbf{M}_{I-1}^p \right)^2 \dots \right. \\ \left. \dots + 2^{p-1} \Delta t_I \mathbf{T}_{I-p-1}^p + \mathbf{M}_{I-p-1}^p \right)^2 + 2^p \Delta t_I \mathbf{K}_{I-p}^p + \mathbf{M}_{I-p}^p.$$

The operator  $\mathbf{E}_I^p$  adapts the time step at each resolution.

## 5.2 Numerical Experiments.

We compare the stability and accuracy of the space and time adaptive scheme with the stability of the space adaptive scheme. Comparisons between the space adaptive scheme and more classical numerical schemes have been done by Liandrat and Tchamitchian [11] so we shall concentrate on the consequences of the time adaptivity. The first set of experiments concerns stability.

### Stability for Burgers equation.

To study the impact of the time adaptivity by itself, we do not introduce any spatial adaptivity and do not apply a threshold to the wavelet coefficients. We choose the initial condition  $u_0(x) = \sin(\pi x)$ . The finest resolution  $2^I$  is normalized to 1 and the finest grid contains 64 coefficients on the interval  $[0, 1]$ . For each scheme there exists a maximum time step  $\Delta t_{max}$  and the scheme is stable if and

	<i>Non Adapt. Time</i>	<i>Time Adapt.</i>
<i>Shannon</i>	$5.37 \times 10^{-3}$	$4.47 \times 10^{-3}$
<i>Meyer</i>	$6.91 \times 10^{-3}$	$5.24 \times 10^{-3}$
<i>Spline 3</i>	$6.41 \times 10^{-3}$	$4.84 \times 10^{-3}$
<i>Spline 5</i>	$5.95 \times 10^{-3}$	$4.68 \times 10^{-3}$
<i>Spline 7</i>	$5.74 \times 10^{-3}$	$4.60 \times 10^{-3}$
<i>Spline 9</i>	$5.62 \times 10^{-3}$	$4.51 \times 10^{-3}$
<i>Daubechies 10</i>	$7.78 \times 10^{-3}$	$5.63 \times 10^{-3}$
<i>Daubechies 14</i>	$7.30 \times 10^{-3}$	$5.08 \times 10^{-3}$
<i>Daubechies 16</i>	$6.76 \times 10^{-3}$	$4.79 \times 10^{-3}$
<i>Daubechies 18</i>	$7.00 \times 10^{-3}$	$5.52 \times 10^{-3}$

Table 3: For each orthogonal wavelet listed in the first column, the second and third columns give the maximum time increment  $\Delta t_I$  for which the nonadaptive in time scheme and the time adaptive scheme are stable, respectively, for Burgers equation. Stability is with the  $L_\infty$  norm of the solution at a given time  $T$ .

only if  $\Delta t_I \leq \Delta t_{max}$ . The stability is tested with the  $L_\infty$  norm of the solution. We know that the solution of Burgers equation satisfies  $\|u(t, x)\|_\infty \leq \|u_0(x)\|_\infty$ . Thus a scheme is unstable if after a certain time  $T$ , the computed solution  $\tilde{u}(T, x)$  satisfies  $\|\tilde{u}(T, x)\|_\infty \geq E\|u_0(x)\|_\infty$  (where  $E$  is a constant greater than 1). We used a dichotomic method to compute the  $\Delta t_{max}$  for both the time adaptive and the forward Adams-Bashforth scheme. We set  $\epsilon = 10^{-2}/\pi$ ,  $p = 5$  (number of octaves, as in (88) and (89)),  $T = 3/\pi$  and  $E = 15$ . The time  $T$  is chosen large enough so that derivatives of the solution reach their largest value before  $T$ . This test was repeated for several wavelets. Table 3 compares the maximum time increment  $\Delta t_I$  for the time adaptive scheme (88) and the corresponding non time adaptive scheme. Contrary to what happens in the case of the heat equation and the linear advection equation, as shown in Tables 1 and 2, Table 3 shows that the maximum time increments are different for the time-adaptive scheme and the non time adaptive scheme. The differences are more important for the Daubechies wavelets but the maximum time increments still remain in the same general range of values for the two schemes.

### Complexity and Accuracy for Burgers equation.

If  $\Delta t_I$  is the global time step for the nonadaptive in time algorithm, we need to iterate  $n = T/\Delta t_I$  times in order to compute the solution at  $t = T$ . Let  $N_I$  be the total number of points that characterize the solution at the resolution  $2^I$ . At time  $k\Delta t_I$ , the number of operations at the resolution  $2^j$  is proportional to the number of nonzero wavelet coefficients  $n_j(k\Delta t_I)$  (after applying a threshold) that characterize the projection of the solution on  $\mathbf{W}_{j-1}$ . Indeed, the number of operations for the operator  $\mathbb{T}_j(f)$  at each time step  $k\Delta t_I$  is still proportional to the number of coefficients that characterize the solution in  $\mathbf{W}_{j-1}$ , as it is for the linear advection equation. As mentioned in Section 3, this is because the nonlinear Burgers operator  $\mathbf{K}$  involves differential operators and a bilinear operation [6]. The number of wavelet coefficients  $n_j(k\Delta t_I)$  changes with the time factor  $k$  because high frequencies are created as time increases (see Fig. 4).

Let us suppose that the wavelet decomposition is computed on  $p$  octaves. The total number of

	<i>Exact</i>	<i>Spatial</i>	<i>Time-Spatial</i> <i>ratio : 2</i>	<i>Time-Spatial</i> <i>ratio <math>\sqrt{2}</math></i>
$L_\infty$ error	–	$2.3 \times 10^{-3}$	$4.2 \times 10^{-3}$	$2.7 \times 10^{-3}$
<i>Slope</i>	1.975	1.995	1.905	1.978
<i>Complexity</i>	–	$10^5$	$3 \times 10^4$	$6 \times 10^4$

Table 4: The first line gives the value of the  $L_\infty$  error of the solutions computed with the spatial but non time adaptive scheme, the space and time adaptive scheme with a time factor of 2, and the space and time adaptive scheme with a time factor of  $\sqrt{2}$ , respectively. The second line gives the value of the slope at the location of the shock. The last line gives the computational complexity using (89) and (90).

operations to compute the solution at time  $T$  with the nonadaptive in time scheme is

$$O \left( \sum_{j=I-p+1}^I \sum_{k=1}^{\frac{T}{\Delta t_I}} n_j(k \Delta t_I) + \frac{T}{\Delta t_I} 2^{-p} N \right). \quad (89)$$

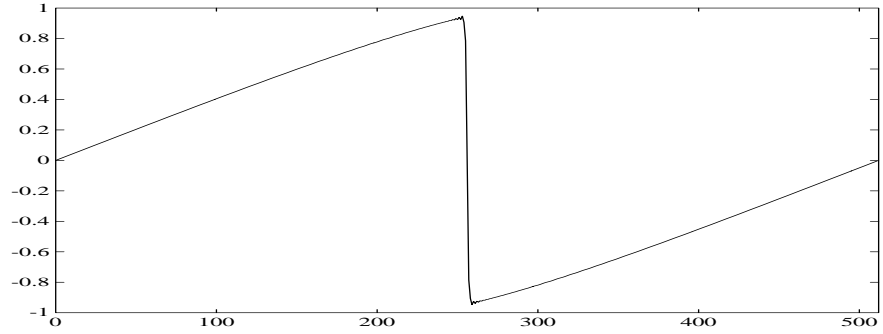
For the time adaptive scheme each resolution  $2^j$  has a specific time step  $\Delta t_j = 2^{I-j} \Delta t_I$  and thus  $2^{j-I} \frac{T}{\Delta t_I}$  iterations are needed. The total complexity is given by

$$O \left( \sum_{j=I-p+1}^I \sum_{k=1}^{2^{j-I} \frac{T}{\Delta t_I}} n_j(k 2^{I-j} \Delta t_I) + 2^{-p} \frac{T}{\Delta t_I} 2^{-p} N \right). \quad (90)$$

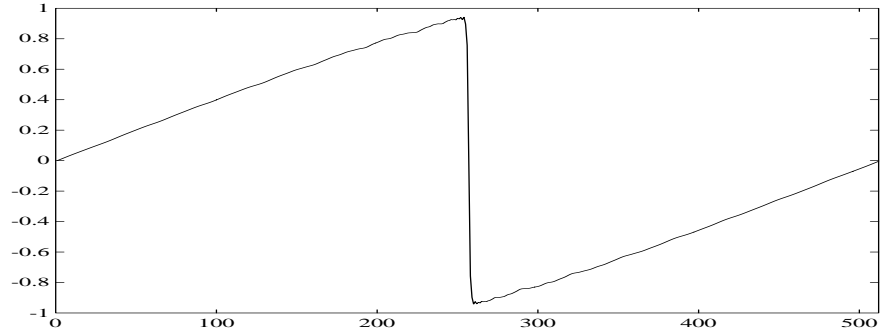
The constants for the complexity in (89) and (90) are approximately the same. In the following numerical experiments, the complexity is computed by evaluating the summations in (89) and (90).

To compare the complexity and accuracy of the space-time adaptive scheme and the space adaptive scheme we computed (for both schemes) the solution of Burgers equation (with  $\epsilon = 2.5 \times 10^{-3}/\pi$ ) at time  $T = 1/\pi$ . In these experiments the wavelet grid has 512 coefficients. The threshold ( $= 2 \times 10^{-2}$ ) has been chosen in order to keep errors comparable to those due to the limitation of the resolution (i.e.,  $\|u_T(x) - \mathbf{P}_{V_0} u_T(x)\|_\infty$  where  $u_T$  is the exact solution at time  $T$ ). Moreover, the time step  $\Delta t_0$  (at the resolution 1) used by both schemes is  $\Delta t_0 = 2.5 \times 10^{-4}$ ; it is the largest time step for which both schemes are stable. For each scheme we measured the  $L_\infty$  error, the value of the slope at the location of the shock and the complexity. These values are displayed in the following table.

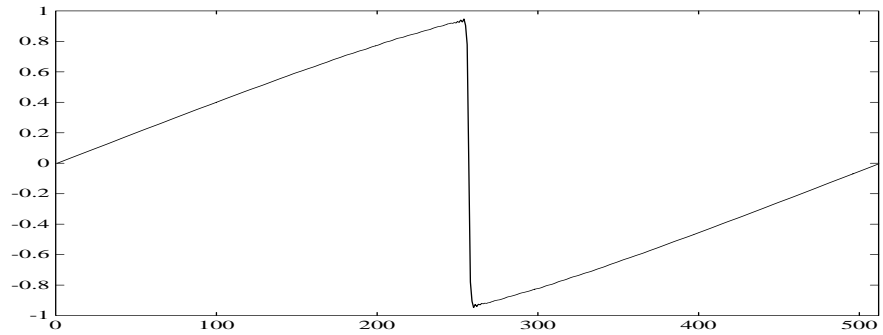
Fig. 5(a) shows the solution at time  $T$ , computed with a spatial adaptive scheme which is not time adaptive. Fig. 6(a) shows the difference between this computed solution with the exact one. Fig. 5(b) shows the solution computed with the spatial and time adaptive scheme and Fig. 6(b) shows the error. Fig. 5(d) gives the wavelet adaptive grid at time  $T$ . Out of 512 coefficients only 128 are “active”. Table 4 shows that the time adaptive algorithm reduces the complexity by a factor 3.3 but introduces more errors. The numerical experiments were performed with the wavelet *spline 7*. We repeated these computations with other spline wavelets and Daubechies wavelets and the numerical results were similar. In the error of the time-adaptive algorithm (Fig. 6(b)), the



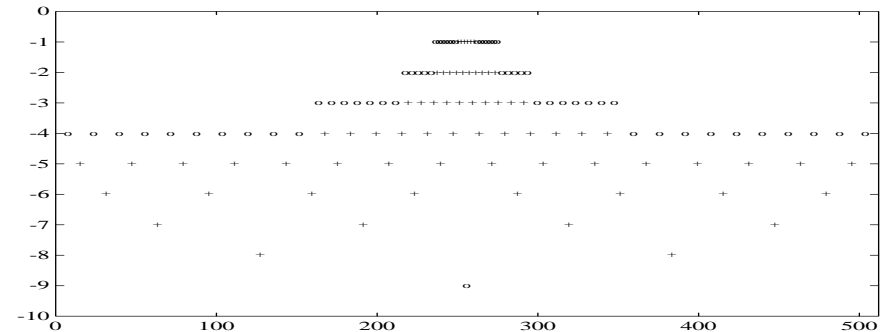
(a)



(b)

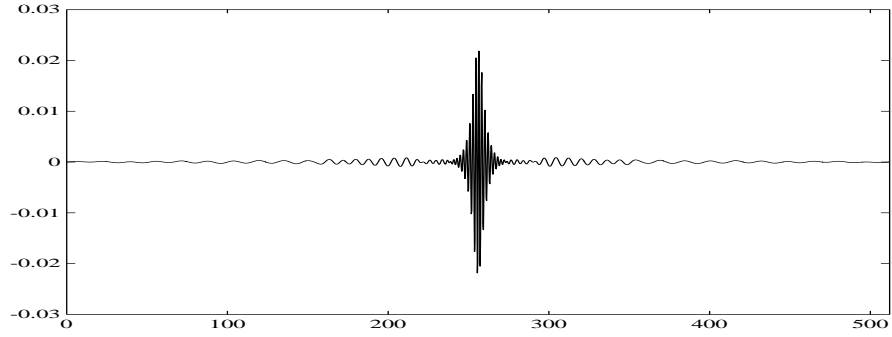


(c)

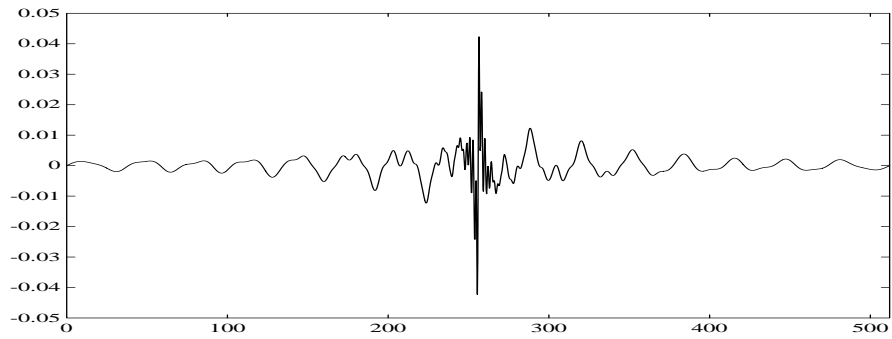


(d)

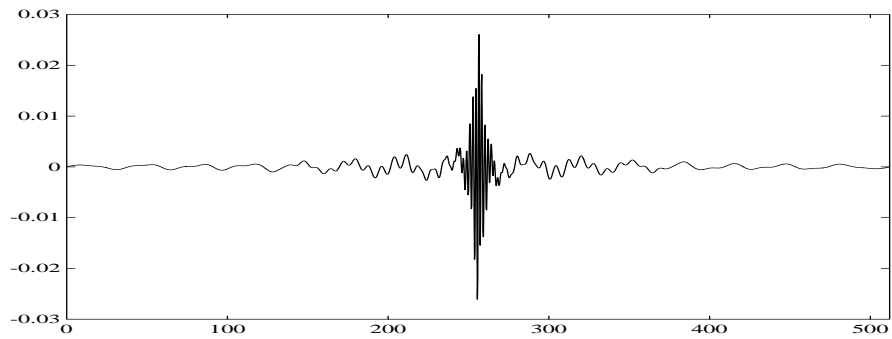
Figure 5: Graph (a) is the solution of Burgers equation computed with the spatial adaptive scheme that is not time adaptive, at time  $T = 1/\pi$ . Graph (b) is obtained with a space and time adaptive scheme, with a time ratio of 2 between two consecutive resolution levels:  $\Delta t_{I+n} = 2^n \Delta t_I$ . Graph (c) is also computed with a space and time adaptive scheme but with a different time ratio:  $\Delta t_{I+2n} = 2^n \Delta t_I$  and  $\Delta t_{I+2n+1} = 2^n \Delta t_I$ . The grid (d) is the adaptive grid of wavelet coefficients of the solution at  $T = 1/\pi$ .



(a)



(b)



(c)

Figure 6: Error curves computed by subtracting the numerical solutions displayed in Fig. 5 from the exact solution of the Burgers equation. The error curves in (b) and (c) correspond to the solutions 5(b) and 5(c) computed with time adaptive schemes. The time adaptive schemes increase the relative proportion of low-frequency errors but the global  $L_\infty$  error in (c) is approximately the same as the error (a) of the nonadaptive in time scheme.

relative amplitude of low-frequencies to high frequencies is much larger than for the nonadaptive in time algorithm. The increase of low-frequency errors is not a problem since the total error is dominated by high frequencies. The basic idea of the algorithm is precisely to have reduction of complexity by introducing more errors at low frequencies as long as these errors remain smaller than the high frequency errors. However, in nonlinear equations, such as Burgers equation, the different frequency bands are not independent. There is an exchange of energy between low and high frequencies because of the nonlinearity of the operator  $\mathbf{K}$ . This is one of the reasons why an increase of errors at low frequencies also increases the errors at high frequencies. To decrease the error in the time adaptive scheme one may simply decrease the time step  $\Delta t_I$  at the finest resolution. Numerical experiments show that if the time step is reduced by a factor of 2 (i.e.,  $\Delta t_0 = 1.25 \times 10^{-4}$ ) the  $L_\infty$  error remains larger than  $3 \times 10^{-3}$  and that the slope is not as close to the exact slope as the one obtained with the space adaptive scheme.

The space-time adaptive scheme that we described has a time step which is inversely proportional to the resolution  $2^j$  because of the advection term of the Burgers equation. With this approach we obtain a scheme which is stable for the same range of time steps  $\Delta t_I$ . However, we introduce more errors at high frequencies due to the exchange of energy between the different frequency bands. Instead of decreasing the time step  $\Delta t_I$  at the finest resolution  $2^I$ , an alternative is to choose a dilation factor between the time steps at different resolutions that is smaller than 2. This enables us to maintain high accuracy at the low frequencies so that we do not increase the high frequency errors through exchange across frequencies. One can easily implement a time adaptive algorithm where the time step increases with a factor of 2 when the resolution is decreased by a factor of 4 (instead of 2). It is as if we had chosen a time ratio of  $\sqrt{2}$  across resolution levels. Let us suppose that the index  $I$  is even, and that the number of octaves  $p$  is also even. We define a scheme where the time step at the resolutions  $2^{2j}$  and  $2^{2j-1}$  is the same and equal to  $2^{\frac{I}{2}-j} \Delta t_I$ :

$$U_I^p(t + 2^{\frac{p}{2}} \Delta t_I, x) = \mathbf{E}_I^p U_I^p(t, x) \quad (91)$$

with

$$\begin{aligned} \mathbf{E}_I^p = & \left( \dots \left( (\mathbf{I}^p + \Delta t_I \mathbf{T}_I^p + \Delta t_I \mathbf{T}_{I-1}^p + \mathbf{M}_I^p + \mathbf{M}_{I-1}^p)^2 \right. \right. \\ & + 2\Delta t_I \mathbf{T}_{I-2}^p + 2\Delta t_I \mathbf{T}_{I-3}^p + \mathbf{M}_{I-2}^p + \mathbf{M}_{I-3}^p \left. \right)^2 + \dots \\ & \dots + 2^{\frac{p}{2}-1} \Delta t_I \mathbf{T}_{I-p+2}^p + 2^{\frac{p}{2}-1} \Delta t_I \mathbf{T}_{I-p+1}^p + \mathbf{M}_{I-p+2}^p + \mathbf{M}_{I-p+1}^p \left. \right)^2 \\ & + 2^{\frac{p}{2}} \Delta t_I \mathbf{K}_{I-p}^p + \mathbf{M}_{I-p}^p. \end{aligned} \quad (92)$$

The number of operations is given by a formula similar to (90)

$$O \left( \sum_{j=\frac{I-p}{2}}^{\frac{I}{2}} 2^{j-\frac{I}{2}} \frac{T}{\Delta t_I} \sum_{k=1}^{2^j-\frac{I}{2}} \left( n_{2j}(k 2^{\frac{I}{2}-j} \Delta t_I) + n_{2j-1}(k 2^{\frac{I}{2}-j} \Delta t_I) \right) + 2^{-\frac{p}{2}} \frac{T}{\Delta t_I} 2^{-p} N \right) \quad (93)$$

The complexity, the  $L_\infty$  error and the slope of the solution obtained with this new time adaptive scheme are shown in the ‘‘Time-Spatial, ratio  $\sqrt{2}$ ’’ column of Table 4. Fig. 5(c) is the graph of the solution computed with this other space-time adaptive scheme and Fig. 6(c) displays the error. As expected, the high-frequency errors are smaller than those of the time adaptive scheme (88) but the low-frequency errors are still higher than for the nonadaptive in time scheme. In this case the amplitude of the high frequency errors remains approximately the same as for the

nonadaptive in time algorithm. We see that the increase of low-frequency errors is not enough to increase substantially the high frequency errors through the exchange of energy across frequencies. Moreover, Table 4 shows that for this new adaptive scheme the value of the slope computed at the location of the shock is as accurate as the result obtained with the space adaptive algorithm. In this case the computational complexity of the time adaptive scheme is approximately half that of the nonadaptive in time algorithm. These results show that by adapting the time ratio between the different spatial resolutions we can keep the same accuracy while decreasing the numerical complexity. The time ratio must not be determined on stability considerations alone. We must also take into account the nonlinear properties of the PDE to maintain a balance between the sources of error.

## 6 Conclusions.

In this paper we present a wavelet based numerical scheme that adapts the space and time resolutions to the properties of the PDE and the local structure of the solution. We showed numerically for the heat equation and the linear advection equation that our time-adaptive scheme is stable for time dilations equal to 4 and 2, respectively. We have no general mathematical proof of this stability although it appears to depend on the multiresolution structure that is behind the wavelet orthonormal bases. One can adapt the time factors in order to keep good accuracy while maintaining stability. For Burgers equation, numerical results indicate that a time factor smaller than 2 does not increase the  $L_\infty$  error of the solution although it decreases the numerical complexity. An important issue is understanding how to adapt the time scaling factor depending upon properties of the nonlinear equation.

Although the time adaptive scheme (equations (42), (71) and (88)) looks more complicated than a nonadaptive time scheme, from a programming point of view, this increase of software complexity is negligible compared to what is needed to implement a spatial adaptive wavelet scheme. We did not go into the details of implementation issues related to the calculation of the different operator  $\mathbf{K}_j$  and  $\mathbf{T}_j$  in a wavelet basis because we focused on the time adaptivity issues. However, although the numerical complexity for applying these operators is linear in the number of nonzero wavelet coefficients, the constants involved are not small, especially when the operator is nonlinear. This is one limitation of wavelet-based numerical schemes and it has been studied by Beylkin [5]. Another problem concerns the treatment of boundaries. No efficient technique has yet been found that includes boundary conditions. However, Meyer [15] as well as Xu and Shann [18] recently found a way to build orthogonal wavelets on finite domains, which can probably help solve these boundary issues. There are still technical difficulties in implementing efficiently wavelet schemes to solve PDE in several dimensions, but we believe that these bases provide a novel approach that will be competitive for PDE like the nonlinear Schroedinger equation [9], that generate solutions with localized structures in space that evolve quickly in time.

**Appendix 1:** *Stability of the time adaptive scheme for the heat equation with Shannon wavelets.*

In this Appendix we prove that the operator  $\mathbf{E}_I^p$  of the wavelet time adaptive scheme for the heat equation (42) satisfies

$$\|\mathbf{E}_I^p\| \leq 1 \iff \|\mathbf{I} + \Delta t_I \mathbf{K}_I\| \leq 1 \quad (94)$$

for Shannon wavelets. The proof is easy because all the operators involved are diagonalized by the Fourier transform. Let us first characterize the spaces  $\mathbf{V}_j$  and  $\mathbf{W}_j$  as well as the operators  $\mathbf{K}_j$  and  $\mathbf{T}_j$  for a Shannon wavelet. One can easily prove that the space  $\mathbf{V}_j$  of the corresponding multiresolution approximation is the space of all functions whose Fourier transforms have support in the interval  $[-2^j\pi, 2^j\pi]$ . The space  $\mathbf{W}_j$  is the set of functions whose Fourier transforms have support in the intervals  $[-2^j2\pi, -2^j\pi] \cup [2^j\pi, 2^j2\pi]$ . For any  $f \in \mathbf{L}^2(\mathbf{R})$ , the Fourier transform of  $\mathbf{P}_{V_j}f(x)$  is  $\hat{f}(\omega)\chi_j^0(\omega)$ , where  $\chi_j^0(\omega)$  is the indicator function of the interval  $[-2^j\pi, 2^j\pi]$ . The Fourier transform of  $\mathbf{P}_{W_j}f(x)$  is  $\hat{f}(\omega)\chi_j^1(\omega)$ , where  $\chi_j^1$  is the indicator function of the interval  $[-2^j2\pi, -2^j\pi] \cup [2^j\pi, 2^j2\pi]$ . For the heat equation,  $\mathbf{K}f(x) = \frac{\partial^2 f(x)}{\partial x^2}$ . Hence, the Fourier transform of  $\mathbf{K}_j f(x)$  is  $-\omega^2 \chi_j^0(\omega) \hat{f}(\omega)$ . The Fourier transform of  $\mathbf{T}_j f(x)$  is  $-\omega^2 \chi_j^1(\omega) \hat{f}(\omega)$ .

The identity operator  $\mathbf{I}$  that appears in the expression of  $\mathbf{E}_I^p$  given in (42) can be replaced by  $\mathbf{P}_{V_I}$  since the initial solution belongs to  $\mathbf{V}_I$  and then remains in  $\mathbf{V}_I$ . Since

$$\mathbf{P}_{V_I} = \sum_{j=I-p}^{I-1} \mathbf{P}_{W_j} + \mathbf{P}_{V_{I-p}}, \quad (95)$$

the operator  $\mathbf{E}_I^p$  becomes

$$\mathbf{E}_I^p = \left( \dots \left( \sum_{j=I-p}^{I-1} \mathbf{P}_{W_j} + \mathbf{P}_{V_{I-p}} + \Delta t_I \mathbf{T}_I \right)^4 + 4\Delta t_I \mathbf{T}_{I-1} \right)^4 + \dots + 4^{p-1} \Delta t_I \mathbf{T}_{I-p-1} \right)^4 + 4^p \Delta t_I \mathbf{K}_{I-p}. \quad (96)$$

For the Shannon wavelet, one can verify that for any  $f(x) \in \mathbf{L}^2(\mathbf{R})$ ,  $\mathbf{T}_j f(x) \in \mathbf{W}_j$ . We thus have the following properties

$$\forall (j, l) \in \mathbb{Z}^2, j \neq l, \mathbf{T}_j \mathbf{T}_l = 0, \quad (97)$$

$$\forall (j, l) \in \mathbb{Z}^2, j \geq l, \mathbf{T}_j \mathbf{K}_l = 0, \quad (98)$$

$$\forall (j, l) \in \mathbb{Z}^2, j \neq l + 1, \mathbf{P}_{W_j} \mathbf{T}_l = 0, \quad (99)$$

$$\forall (j, l) \in \mathbb{Z}^2, j \geq l, \mathbf{P}_{W_j} \mathbf{K}_l = 0. \quad (100)$$

As a consequence, since all the operators in equation (96) commute, the operator  $\mathbf{E}_I^p$  simplifies to

$$\begin{aligned} \mathbf{E}_I^p &= (\mathbf{P}_{W_{I-1}} + \Delta t_I \mathbf{T}_I)^{4^p} + (\mathbf{P}_{W_{I-2}} + 4\Delta t_I \mathbf{T}_{I-1})^{4^{p-1}} + \dots + (\mathbf{P}_{W_{I-p}} + 4^{p-1} \Delta t_I \mathbf{T}_{I-p+1})^4 \\ &\quad + \mathbf{P}_{V_{I-p}} + 4^p \Delta t_I \mathbf{K}_{I-p}. \end{aligned} \quad (101)$$

Since for different  $k$ , the operators  $\mathbf{P}_{W_{I-k-1}} + 4^k \Delta t_I \mathbf{T}_{I-k}$  and  $\mathbf{P}_{V_{I-p}} + 4^p \Delta t_I \mathbf{K}_{I-p}$  act on mutually orthogonal spaces,  $\|\mathbf{E}_I^p\| \leq 1$  if and only if for any  $k < p$

$$\|\mathbf{P}_{W_{I-k}} + 4^k \Delta t_I \mathbf{T}_{I-k}\| \leq 1, \quad (102)$$

and

$$\|\mathbf{P}_{V_{I-p}} + 4^p \Delta t_I \mathbf{K}_{I-p}\| \leq 1. \quad (103)$$

From the expression of  $\mathbf{T}_j$  and  $\mathbf{K}_j$  in the Fourier domain, for any  $\Delta t_I$  and  $k < p$ , one can show that

$$\|\mathbf{P}_{W_{I-k}} + 4^k \Delta t_I \mathbf{T}_{I-k}\| \leq 1 \iff \|\mathbf{P}_{V_{I-p}} + 4^p \Delta t_I \mathbf{K}_{I-p}\| \leq 1 \iff \|\mathbf{I} + \Delta t_I \mathbf{K}_I\| \leq 1. \quad (104)$$

We thus obtain

$$\|\mathbf{E}_I^p\| \leq 1 \iff \|\mathbf{I} + \Delta t_I \mathbf{K}_I\| \leq 1. \quad (105)$$

## Appendix 2: Stability of the linear advection time-adaptive scheme for the Shannon wavelet.

In this Appendix we prove that the time adaptive scheme defined by the operator

$$\begin{aligned} \mathbf{E}_I^p = & \left( \dots \left( (\mathbf{I} + \Delta t_I \mathbf{T}_I^p + \mathbf{M}_I^p)^2 + 2\Delta t_I \mathbf{T}_{I-1}^p + \mathbf{M}_{I-1}^p \right)^2 + \dots + 2^{p-1} \Delta t_I \mathbf{T}_{I-p-1}^p + \mathbf{M}_{I-p-1}^p \right)^2 \\ & + 2^p \Delta t_I \mathbf{K}_{I-p}^p + \mathbf{M}_{I-p}^p \end{aligned} \quad (106)$$

is stable over the same range of time steps  $\Delta t_I$  as the non time adaptive scheme. Let us first state a few properties of the usual Adams-Bashforth scheme. For the operator  $\mathbf{K} = \frac{\partial}{\partial x}$ , the Adams-Bashforth scheme is defined by

$$u(t + \Delta t, x) = u(t, x) + \Delta t (a \mathbf{K}u(t, x) + b \mathbf{K}u(t - \Delta t, x) + c \mathbf{K}u(t - 2\Delta t, x)), \quad (107)$$

with  $a = 23/12$ ,  $b = -16/12$ ,  $c = 5/12$ . If the initial condition  $u_0(x)$  has a Fourier transform included in an interval  $[-\omega_m, \omega_m]$ , the scheme is stable if and only if

$$\omega_m \Delta t \leq C, \quad (108)$$

where  $C$  is a constant independent of  $\omega_m$ . For the Shannon wavelet the operator  $\mathbf{K}_I$  is a restriction of  $\mathbf{K}$  to the space  $\mathbf{V}_I$  which corresponds to the frequency interval  $[-2^I \pi, 2^I \pi]$ . Thus, the numerical scheme

$$\tilde{u}_I(t + \Delta t_I, x) = \tilde{u}_I(t, x) + \Delta t_I (a \mathbf{K}_I \tilde{u}_I(t, x) + b \mathbf{K}_I \tilde{u}_I(t - \Delta t_I, x) + c \mathbf{K}_I \tilde{u}_I(t - 2\Delta t_I, x)) \quad (109)$$

is stable if and only if  $\Delta t_I \leq (C/\pi)2^{-I}$ . Similarly, the operator  $\mathbf{T}_{I-k}$  is a restriction of  $\mathbf{K}$  to the frequency intervals  $[-2^{I-k+1}2\pi, -2^{I-k+1}\pi] \cup [2^{I-k+1}\pi, 2^{I-k+1}2\pi]$ . Thus, the numerical scheme

$$\begin{aligned} \mathbf{P}_{W_{I-k+1}} \tilde{u}_I(t + 2^k \Delta t_I, x) = & 2^k \Delta t_I (a \mathbf{T}_{I-k} \tilde{u}_I(t, x) + b \mathbf{T}_{I-k} \tilde{u}_I(t - 2^k \Delta t_I, x) + c \mathbf{T}_{I-k} \tilde{u}_I(t - 2^{k+1} \Delta t_I, x)) \\ & + \mathbf{P}_{W_{I-k+1}} \tilde{u}_I(t, x) \end{aligned} \quad (110)$$

is stable if and only if  $\Delta t_I \leq (C/\pi)2^{-I}$ . As we shall see, the stability of  $\mathbf{E}_I^p$  is based on these properties.

We decompose each component of  $U_I^p(t, x)$  into the different spaces  $\mathbf{W}_j$  which correspond to disjoint frequency intervals. We define the operators

$$\mathbf{P}_{W_j} U_I^p(t, x) = \begin{pmatrix} \mathbf{P}_{W_j} \tilde{u}_I(t, x) \\ \mathbf{P}_{W_j} \tilde{u}_I(t - 2\Delta t_I, x) \\ \vdots \\ \mathbf{P}_{W_j} \tilde{u}_I(t - 2^{p+1} \Delta t_I, x) \end{pmatrix} \quad (111)$$



## References

- [1] R. Bank, "A multilevel iterative method for nonlinear elliptic equations", *Elliptic Problem Solvers*, M. Schultz, Ed., p. 1, Academic Press, New York, 1981.
- [2] G. Battle, "A block spin construction of ondelettes". *Communications of Mathematical Physics*, vol. 110, p. 601, 1987.
- [3] M. Berger and P. Colella "Local adaptive mesh refinement for shock hydrodynamics", *Journal of Computational Physics*, vol 82, p. 64-84, 1989.
- [4] M. Berger and J. Olinger, "Adaptive Mesh Refinement for Hyperbolic Partial Differential Equations" *Journal of Computational Physics*, vol. 53, no. 3, p. 484-512, March 1984.
- [5] G. Beylkin, "On the representation of operators in bases of compactly supported wavelets", *Proceedings de l' Ecole sur des Problemes non Lineaires Appliques*, INRIA, Paris, France, June 1991.
- [6] G. Beylkin, R. Cofiman and V. Rokhlin, "Fast wavelet transform and numerical algorithms", *Yale University Tech. Report YALE/DCS/RR-696*, August 1989.
- [7] A. Brandt *Mathematical Computing*, vol. 31, p. 333, 1977. New York, 1981.
- [8] I. Daubechies, "Orthonormal bases of compactly supported wavelets", *Communications in Pure and Applied Mathematics*, vol. 41, p. 909-996, Nov. 1988.
- [9] B. LeMesurier, G. Papanicolaou, G. Sulem and P. Sulem, "Local structure of the self focusing singularity of the nonlinear Schroedinger equation", *Physica D*, vol 32, p. 210-226, 1988.
- [10] P.G. Lemarie, "Ondelettes a localisation exponentielles", *Journal de Mathematiques Pures et Appliquees*, 1988.
- [11] J. Liandrat and Ph. Tchamitchian, "Resolution of the 1D regularized Burgers equation using a spatial wavelet approximation", NASA Report, ICASE Report. no. 90-83, Dec. 1990.
- [12] S. Mallat, "Multiresolution approximation and wavelet orthonormal bases of  $L^2$ ", *Trans. of the American Mathematical Society*, vol. 315, p. 69-87, Sept. 1989.
- [13] S. Mallat, "A theory for multiresolution signal decomposition : the wavelet representation", *IEEE Trans. on Pattern Analysis and Machine Intelligence*, vol. 11, no. 7, p. 674-693, July 1989.
- [14] Y. Meyer "Ondelettes et operateurs", Hermann, 1990.
- [15] Y. Meyer "Ondelettes orthogonales sur un interval", preprint CEREMADE, Universite Paris Dauphine, 1991.
- [16] V. Perrier and C. Basdevant, "La decomposition en ondelettes periodiques, un outil pour l'analyse des champs inhomogenes. Theorie et algorithmes," *La Recherche Aerospatiales*, no. 3, p. 53-67, 1989.
- [17] J. Stromberg "A modified Franklin system and higher-order systems of  $R_n$  as unconditional bases for Hardy spaces", *Conference in Harmonic Analysis in Honor of A. Zygmund*, vol. 2, p. 475-493, edit. W. Beckner et. al., Wadsworth Math. Series.

- [18] J.-C. Xu and W.-C. Shann, “Galerkin-wavelets Methods for Two-point Boundary Value Problems”, preprint, May 1991.
- [19] H. Yserentant, “On the multi-level splitting of finite element spaces”, *Numeri. Math.* vol. 49, p. 379-412, 1986.